Synthesis and use of Janus SiO_2 nanoparticles for formulating model heavy oil macroemulsions

D. Fabio Mercado[1], Luz M. Ballesteros-Rueda[1], Cindy C. Lizarazo Gómez[1], Brucxen E. Núñez Rodríguez[1], Edward Arenas-Calderón,[1] Víctor G. Baldovino-Medrano[1,2*]

[1]Centro de Investigaciones en Catálisis (@CICAT UIS), Parque Tecnológico Guatiguará (PTG), Universidad Industrial de Santander, Km. 2 vía El Refugio.

[2]Laboratorio de Ciencia de Superficies (@Csss UIS), Parque Tecnológico Guatiguará (PTG), Universidad Industrial de Santander, Km. 2 vía El Refugio, Piedecuesta (Santander) 681011, Colombia

E-mail: vicbaldo@uis.edu.co

ABSTRACT

Janus nanoparticles have applications in many fields. Particularly, the oil industry is interested in applying them for enhanced oil recovery. Within this context, there is a need to understand the influence of the factors involved in the formulation of crude oil type emulsions over their properties and rheological behavior. In this contribution, spherical SiO_2 Janus nanoparticles of two different sizes were synthesized and used as surfactants for the formulation of aqueous emulsions with two model oils: namely, squalane and vacuum gas oil. Factorial experiments were designed and made to analyze the effects of the particle size of the Janus nanoparticles, the water content, the emulsification energy, and of the second and third order interactions between these variables over the droplet size distributions, polydispersity, and rheological profiles of the emulsions. On the one hand, it was found that the used Janus nanoparticles produced either water in oil (for vacuum gas oil) or oil in water (for squalane) depending on the chemistry of the oil phase. On the other hand, it was demonstrated that non-additive factors

play an important role over the properties of the emulsions; especially in the case of the water in oil ones. These effects also implied non-additive correlations between the droplet size distributions of the emulsions and their rheological behavior. Therefore, this work demonstrates that simpler linear relationships do not suffice for finding the best conditions for formulating crude oil type emulsions aimed for applications such as enhanced oil recovery.

KEYWORDS: SiO_2 based Janus nanoparticles, enhanced oil recovery, formulation of emulsions, non-additive effects, rheology.

1. INTRODUCTION

Emulsions have applications in drug delivery,[1] cosmetics,[2] food,[3] petroleum industry[4], etcetera.[5] An emulsion is a heterogeneous system that consists of at least one immiscible liquid; the dispersed phase, forming droplets in another; the continuum phase. Typical emulsions are classified as oil-in-water (O/W), when water is the continuum phase, and as water-in-oil (W/O), in the opposite case. The size of the droplets of the dispersed phase is another criterium to classify emulsions. Therefore, microemulsions are said to be made of droplets whose sizes are between 5 and 100 nm, while macroemulsions are made of droplets of larger sizes. Micro- and macroemulsions also differ in terms of their stability;[6] namely, the former are thermodynamically stable, whereas the latter are thermodynamically unstable and require a considerable input of kinetic energy for their formation.[7]

The use of additives for achieving stability for macroemulsions is common practice.[8–10] The additives are typically molecules, called surfactants, with an amphiphilic behavior, i.e., their structure has both lipophilic and hydrophilic segments, which facilitate their interaction with both phases of the emulsion. Surfactants tend to segregate into the liquid-liquid interface hence decreasing the interfacial surface tension of the system.[11] The phase in which the surfactant is most

soluble ends up being the continuous phase of the emulsion.[6] Hence, the combination of a specific surfactant with a given solvent favors the formation of a specific kind of emulsion (W/O or O/W). Surfactants can also slow down the processes that lead to the breaking of a macroemulsion. For example, surfactants may decrease the rate of coalescence of the dispersed phase by creating mechanical, steric, or electrostatic barriers around its droplets.[12]

The use of solid surfactants based on micro- and nanoparticles has been intensively investigated. The stabilization of emulsions by solids acting as surfactants was discovered by Ramsden[13] and popularized by Pickering.[14] Many particles must be superficially modified to provide them with an amphiphilic character if they are aimed to be used as surfactants.[15] For this purpose, coating agents, i.e., molecules (organic or inorganic) and even smaller particles are adsorbed onto the material to modify its surface physicochemical properties. This process is commonly called functionalization.[16] Without suitable functionalization, nanomaterials often tend to agglomerate once suspended in a liquid.[17,18]

A conventional functionalization process consists of suspending the solid in a solution containing the desired coating agent. The process must be carried out under conditions at which chemisorption of the coating agent over the nanoparticles occurs.[19] Anisotropically functionalized nanomaterials act as Pickering emulsion stabilizers owing to their amphiphilicity.[20] In the literature, amphiphilic materials might be of the "Janus" type when they are provided with two functionalities on their surface as of making allusion to the two-faced Roman god.[19]

Janus nanomaterials have been proposed for applications in biology,[21] the production of nanomotors,[22] catalysis,[22] bioimaging,[22] drug delivery[23–25], and in the oil industry.[26,27] For the latter, Janus nanomaterials are thought to have potential applications in the exploration, drilling, corrosion control, oil-well cementing, enhanced oil recovery, wastewater treatment, and

desulfurization of crude oils.[4,21,23–25,27,28] In the specific case of their application to enhanced oil recovery, an emulsion of Janus nanoparticles must be formulated and injected into the given oil well. Nevertheless, some characteristics of the emulsions such as different nature (W/O or O/W) or the droplet size distribution might impact their performance regardless of the application. Particularly, the properties of macroemulsions strongly depend on the synthesis conditions due to their thermodynamic instability.[29]

There is evidence on the effect of some formulation parameters over the droplet size distribution of macroemulsions; namely, the types of soluble surfactant and oil, the water to oil ratio, the surfactant concentration, the mechanical mixing conditions, the temperature, and, in the case of emulsions from the oil industry, the concentration of brine. Salager et al.[30] studied how the water to oil ratio influences the droplet size distributions of emulsions formulated with a hydrocarbon distillation cut of low viscosity and a heavy crude oil. The authors found that this input variable has a volcano type effect over the average droplet size of the emulsions. Other authors[31,32] found similar effects for emulsions formulated with bitumen. These studies were made for emulsions formulated with soluble surfactants. Regarding Pickering emulsions, there are reports considering the individual effects of solid particle content,[33] particle size,[34] and oil/water volume fraction[35] over the characteristics of emulsions. However, there are very few studies analyzing the possible non-additivity; i.e. interactions, of the effects of the factors involved in the formulation of Pickering emulsions. In this sense, Pey et al.[29] showed that non-additive effects between the factors involved in the formulation of oil, liquid paraffin, in water nano-emulsions play a significant role over their droplet size distribution.

Considering the above, this contribution studies the properties of macroemulsions formulated with SiO_2 Janus nanoparticles, water, and two oil phases relevant for applications in

the oil industry; namely, squalane and vacuum gas oil. The methodology of the research comprised the synthesis of SiO_2 nanoparticles of two different sizes, their further functionalization with a hydrophobic organic coating agent, namely, 3-aminopropyl trimethoxysilane (APTES), following the conventional functionalization pathway and the Pickering emulsion-based method to produced Janus nanoparticles, and further use as surfactant during the formulation of the macroemulsions. Factorial experiments were designed and executed for formulating the emulsions considering the following input variables: the nature of the oil phase of the emulsion: the diameter of the functionalized solid used as surfactant, the volumetric water percentage, and the applied emulsification energy. The influence of these variables and their interactions over the nature, droplet size distribution, and rheological profile of the produced emulsions was assessed.

Materials and methods

Reactants. Milli-Q water (18MΩ·cm at 25°C), tetraethyl orthosilicate (TEOS) 99% wt, 25% ammonium hydroxide, ethanol, 99.5% wt, cetyltrimethylammonium bromide (CTAB) 98% wt, 3-aminopropyl trimethoxysilane (APTES) 98% wt, dichloromethane 99.9% wt, n-heptane 99% wt, squalane 99% wt, sulfuric acid 97%, potassium nitrate 99%, paraffin wax (51-53°C and $\rho = 0.9$ g/mL) and squalane 98% were all supplied by Merck and used without further purification. A sample of a refined vacuum gas oil (VGO) was gently provided by Ecopetrol (Colombia).

Synthesis of SiO_2 nanoparticles. A modification of the method proposed by Stöber et al.[37] was used to produce SiO_2 nanoparticles of two different sizes. Briefly, 200 mL of an aqueous solution containing ethanol (11.80 M) and ammonium hydroxide (0.3M) was prepared and heated at 50°C or 60°C, depending on the desired diameter of the nanoparticles. After the desired temperature was reached, 65 mL of TEOS were added dropwise. The obtained suspension was kept at the same temperature for 1 h. Then, the SiO_2 nanoparticles were separated from the liquid

by centrifugation and washed with water and ethanol twice before drying them at 60°C and 175 mbar for 12 h. The functionalized nanoparticles were suspended in deionized water under ambient conditions. Finally, the nanoparticles were lyophilized for 24 h to remove water (model 79340-022, Labconco equipment). The recovered powder was branded as SiO_2-d_p. Where, d_p is the average diameter of the produced nanoparticles.

Functionalization of the SiO_2 nanoparticles. Two different functionalization protocols were applied. The Pickering method was used to promote anisotropic functionalization.[38] The obtained SiO_2 nanoparticles (400 mg) were well-dispersed in 60 mL of ethanol/water (6.7% w/w) by using a magnetic stirrer. To facilitate the adsorption of the nanoparticles into the oil-water interphase, an adequate amount of CTAB was added to the suspension to obtain a 1.8 mM concentration of the surfactant (this concentration was higher than the critical micellar concentration),[39] and the obtained suspension was heated to 65°C. Finally, ~1.0000 g of solid wax was added to the suspension. After the wax melted, the resulting suspension was kept at the same temperature for 10 min, and then it was shaken in a dispersing instrument (IKA T-25, Ultra Turrax Digital High-Speed Homogenizer (Cole-Parmer®)) at 12000 rpm for 3 min. Then, the system was cooled down under magnetic agitation to room temperature to solidify the wax while producing well-dispersed droplets of paraffin. The functionalization of the unprotected surface of the silica particles was then achieved by mixing the emulsion with an equal volume of an ethanol/water solution containing ammonium hydroxide (7% v/v) and APTES as in agreement with the method presented by Perro et al.[40] The reaction system was kept in agitation at 750 rpm for 12 h. After that time, the solid was separated from the liquid by centrifugation and washed with ethanol to remove physically adsorbed APTES and any other residua. Then, the solid was washed thrice with dichloromethane to remove the residual paraffin from its surface. As a reference, conventional

isotropic functionalization of SiO_2 was performed following the same conditions mentioned above, but without using CTAB and paraffin wax. The functionalized materials are denoted from here as SiO_2-d_p@Anisotr and SiO_2-d_p@Isotr as in regards to the anisotropic and isotropic functionalization, respectively.

Particles characterization. The morphology of the SiO_2 nanoparticles was studied by scanning electronic microscopy (SEM) using an FEI Quanta 650 FEG instrument operated at an electron voltage of 10.00 kV. Previous to the measurements, the samples were dispersed in ethanol, and some drops were added into a carbon-based tape. The images were analyzed with the ImageJ2 software[41] using the individual diameter of at least 250 particles.

Particles surface area and porosity. N_2 adsorption−desorption isotherms at 77 K were measured in a 3FLEX Micromeritics apparatus. The analysis was performed on the SiO_2 materials before their functionalization. In general, 0.15−0.25 g of sample were outgassed overnight at 373 K for 12 h under a vacuum pressure of 15 Pa before running the analyses. The relative pressure (P/P_0) range of the measurements was comprised between 0.01−0.99 with 59 points being collected to complete the isotherms. The BET specific surface area (SS_{BET})[42] of the materials was computed by using data within the linear range of relative pressures between 0.04 and 0.24 according to IUPAC recommendations.[43]

Assessment of the surface chemistry of the materials. The functional groups present in the nanoparticles were identified by their infrared (IR) signals using a Thermo Scientific™ Nicolet™ iS™50 spectrometer working at 128 scans that were averaged at a 2 cm^{-1} resolution within the range 4000-400 cm^{-1}. The solids were diluted with KBr and then analyzed. To analyze the effect of temperature on the IR signals, samples were put inside a vacuum chamber coupled to the

spectrometer, and they were heated from 50 up to 800 °C using a 10 °C min^{-1} heating ramp and 10 min of stabilization in the desired final temperature.

Thermogravimetric profiles. Thermogravimetric analysis (TGA) measurements were performed with a Discovery series TGA, TA Instruments, interfaced to a computer and controlled by the software TRIOS®. The analyses were performed under a 10 mL/min of nitrogen (99.999%) starting at an initial temperature of 100°C, equilibration time of 10 min, followed by heating to 800°C at a rate of 5°C/min.

Hydrodynamic particle size and Z potential. The hydrodynamic diameter of the particles was measured by dynamic light scattering (DLS) using a LiteSizer 500 instrument, Anton Paar, working at an angle of 15° at (25.0 ± 0.1) °C. The instrument was coupled to a Metrohm automatic titrator, provided with an 867-pH module and an 846 Dosing Interface, working at pH steps of 0.5. The initial pH for these measurements was ca. 12, and the final was ca. 1. A pH-stabilization time of 5 min per step was programmed to measure the Z potential as a function of pH. The runs were performed on aqueous suspensions of the corresponding materials (0.15% w/w) using KNO_3 as background electrolyte. In all cases, the Kalliope™ software was used to control the instrument.

Hydrophobicity. The hydrophobic character of the materials was evaluated by static contact angle measurements. For this purpose, five drops of aqueous suspensions of equal concentration of all materials were deposited over glass slides and then heated up to 140°C until evaporating the solvent. This process was repeated until the formation of a homogeneous layer of the material over the surface, and then the measurement was done. A Drop Shape Analyzer DSA25E instrument controlled by the ADVANCED® software, KRÜSS, was used. The baseline was detected automatically by the equipment. The measurements were made according to a Young-Laplace fit.[44] All measurements were done by triplicate for each material.

Formulation of emulsions. All materials were used as emulsion stabilizers using squalane or vacuum gas oil as oil phase and water in glass test tubes. The selected particles were dispersed in water using an ultrasonic bath (Elmasonic E30H) working at a 37 kHz for 15 min before adding the corresponding oil phase to the aqueous suspension. The obtained mixture was stirred at 300 rpm for 15 min, and finally, the pH was adjusted between 2 – 3 by using H_2SO_4. The emulsions that were physically stable for more than one day were characterized as described next. A particular experimental design was purposely planned and executed for analyzing the characteristics of the emulsions made with the APTES anisotropic functionalized silica nanoparticles. Specifically, the effects of key variables for the formulation of the emulsions; namely, the nature of the oil phase of the emulsion: squalane or vacuum gas oil, the SiO_2 particle diameter (d_p), the volumetric water percentage (W% [vol.%]), and the applied emulsification energy (ε), see **Section S1.1** for details on the calculation of ε, and of their interactions on their droplet size distributions and rheology were investigated. Therefore, two blocks of a complete 2^3 factorial design were planned and executed. The two experimental blocks were water-squalane and water-vacuum gas oil. The levels of the main variables were d_p = 58 and 88 nm -as from particle size distributions, see **Results** section-, W% = 24.6 and 49.3%, and ε = 4.0 and 13.0 GW/m^3 for the water-squalane emulsions and 4.8 and 16 GW/m^3 for the water-vacuum gas oil emulsions. The concentration of the nanoparticles was 1.48 wt.% in all cases. The statistical analysis of the data was made adopting techniques presented in experimental design textbooks[45,46] and in previous works.[47]

Characterization of the emulsions

Nature. The nature of the emulsions, W/O or O/W, was determined by measuring their conductivity with a research-grade bench meter HI5522 (HANNA® instruments). Further confirmation of these results was made by making drop dissolution tests. For this purpose, some

drops from the emulsions were added to 60 mL of water. If the drops dissolved, the emulsion was classified as of the oil in water type and viceversa if the drops did not dissolve.

Droplets size distributions. Droplets size distributions were measured with the instruments mentioned before using the DLS technique described previously. Measurements were made at 90°. The $D_{90\%}$, $D_{50\%}$ and $D_{10\%}$ diameters were used to calculate the polydispersity of the distributions as shown in equation 1:

$$P = \frac{D_{90\%} - D_{10\%}}{D_{50\%}} \quad \textit{Equation 1.}$$

Where, $D_{X\%}$ denotes the diameter in which X% of the particles have at most the mentioned diameter. These analyses were repeated twice for each one of the formulated emulsions. For the measurements, samples were prepared as previously mentioned for the SiO_2 nanoparticles, but for the vacuum gas oil-water emulsions, n-dodecane was used as dispersant instead. Moreover, a glass cell was used in this instance.

Rheology of the formulated emulsions. Rheological measurements were carried out at 25 °C with an instrument, Paar Physica MCR 301, provided with a cone and plate geometry, CP75-1; cone angle = 0.0175 rad, gap width = 0.5 mm. Measurements were made by ramping up the shear rate (g) from 0.01 to 1000 s^{-1} in 50 steps. The stabilization time at each step was 15 s. Reference tests were performed with water, squalane, and the vacuum gas oil and with a 1.48 wt.% suspensions of the amphiphilic nanomaterials in the squalene or the vacuum gas oil.

2. Results and discussion

In this section, the results of the characterization of all materials, starting with the SiO_2 nanoparticles produced with two different sizes are presented first. Then, the isotropic and

anisotropic functionalization of the SiO_2 nanoparticles to produce four different materials is analyzed. Finally, the properties of the emulsions produced with the anisotropic functionalized materials is discussed.

Characterization of the silica particles. Figure S1 shows SEM images of samples from the silica particles synthesized at 50 and 60°C. The synthesized particles were spherical with very uniform sizes. The means of the particle sizes were: $87.6 \leq \mu_{50°C}[nm] \leq 88.6$ and $57.4 \leq \mu_{60°C}[nm] \leq 58.3$, considering t-Student 99.0% confidence intervals with 265 and 302 degrees of freedom, respectively**. Figure S2** shows that these confidence intervals comply with statistical principles since a normal distribution fits data adequately.[45] The particles synthesized at 50°C were ca. 34% larger than those synthesized at 60°C. DLS measurements shown in **Figure S3** were in line with the values obtained by SEM; namely, these measurements produced volume based mean diameters of 60 ± 4 and 89 ± 3 nm for SiO_2-58 and SiO_2-88, respectively. Considering these results, in what follows, both type of particles will be referred to by replacing d_p in the designated SiO_2-d_p nomenclature by the average particle size of each set of particles; namely, the particles synthesized at 50°C will be named as SiO_2-88, and those synthesized at 60°C will be named as SiO_2-58.

Figure S4 shows the N_2 adsorption isotherms for SiO_2-58 and SiO_2-88. According to the IUPAC classification,[43] these corresponded to a type II isotherm typical of unrestricted monolayer-multilayer adsorption on non-porous materials. Applying the BET model,[42] the estimated specific surface areas, SS_{BET}, for SiO_2-88 and SiO_2-58 were 30.0 (C_{BET} = 222.2) and 33.9 m^2/g (C_{BET} = 214.1), respectively. Therefore, taking SiO_2-88 as a reference, the ~34.1% decrease in the average particle size of SiO_2 led to ~13.3% increase in SS_{BET}. According to what is observed in the isotherms, the surface area of these powders are due to their particle size and not to the development of micro- or mesopores, also called internal porosity. Indeed, an estimation of the

surface area, using the average particle sizes as measured by both SEM and DLS and considering spherical particles with a density of 2.196 cm^3/g,[52] gave values of specific surface area which were very close to those estimated by the BET model; SS_{SEM} ~31.1 and 47.1 m^2/g and SS_{DLS} ~30.7 and 45.5 m^2/g for SiO_2-88 and SiO_2-58, respectively.

Analysis of the functionalized materials. Samples of SiO_2-88 and SiO_2-58 were functionalized with APTES following the protocol mentioned in the experimental section. FTIR spectra for samples of SiO_2-88 and SiO_2-58 and the correspondingly anisotropically functionalized materials are shown in **Figure S5**. For the silica samples, the recorded peaks, **Table S1**, corresponded to the vibrational modes of siloxanes, Si-O-Si, surface silanols, Si-OH, and Si-O-H structures due to physisorbed water.[53,54] Samples from SiO_2-88@Anisotr and SiO_2-58@Anisotr showed two additional peaks around ~2916 and ~2860 cm^{-1} due to the C-H stretching mode from the hydrocarbon structure of the APTES molecule.[55] The band for the N-H group from APTES, expected at ~3400 cm^{-1}, was not observed most likely because of the masking of the broad band attributable to O-H.[56] To get further confirmation of the functionalization of the materials with APTES, temperature-programmed FTIR spectra were recorded for a sample of SiO_2-58@Anisotr. **Figure 2** summarizes these results.

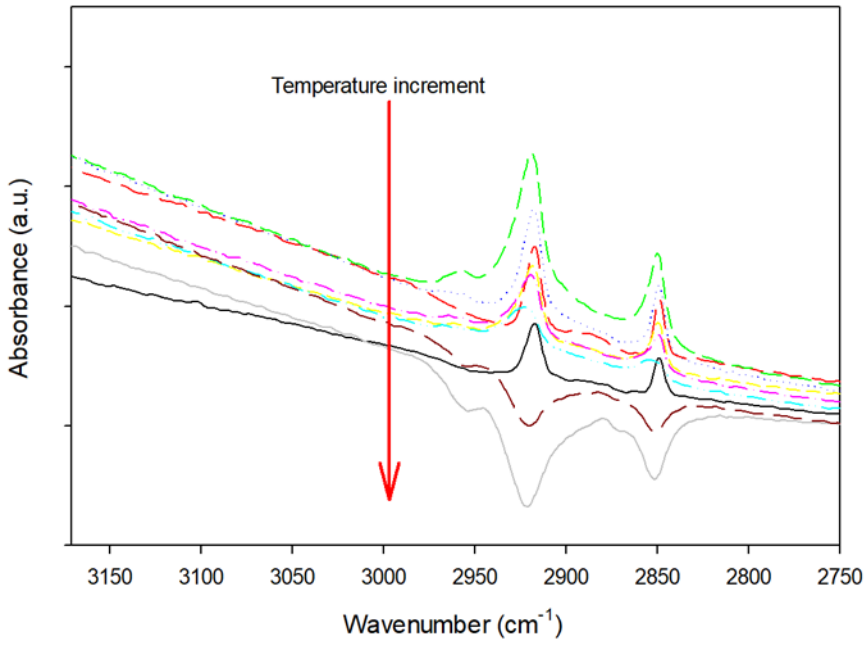

Figure 2. Evolution of the IR spectra from the C-H region of the sample SiO_2-58@Anisotr over a temperature gradient. The corresponding temperatures were 80, 100, 120, 150, 180, 200, 215, 225, and 250°C.

The bands corresponding to the C-H bonds, i.e., those located at ~2916 and ~2860 cm^{-1}, remained stable up to 215°C. Further disappearance of these bands at 225°C was ascribed to desorption since APTES boils at 217°C at 1.0 atm.[52] The ensemble of the FTIR results demonstrates that APTES was chemisorbed over the silica particles hence proving that the functionalization of the silica nanoparticles was successful. Further proof of the functionalization of the silica nanoparticles with APTES was provided by ζ-potential and static contact angle measurements, **Figure 3** and **Table 1.** The ζ–potential profiles of the SiO_2-88 and SiO_2-58 materials as a function of pH were typical of the behavior of SiO_2 in aqueous suspensions.[57] At pH values higher than 8.0, both materials showed a ζ = -52 mV. Decreasing the pH resulted in an increase of ζ, and at pH values around 2.9 with both materials reaching their isoelectric point, IEP, (ζ = 0 mV). The reported IEP for SiO_2 is around 3.0,[58] which agrees with the results presented herein.

Concerning the functionalized materials, the samples from SiO_2-88@Isotr and SiO_2-58@Isotr shifted their isoelectric points from a pH of 2.7 to 7.8 as compared to the corresponding silica nanoparticles, **Table 1**. Notice that the isoelectric point of the isotropically functionalized materials did not change for the two different particle sizes of the silica nanoparticles. This is coherent with a full coverage of the surface of the silica nanoparticles with APTES in both instances. The shifts observed in the IEP of the materials can be attributed to the protonation of the $-NH_2$ groups of APTES into $-NH_3^+$.[57] For the anisotropically functionalized materials, SiO_2-88@Anisotr and SiO_2-58@Anisotr, the isoelectric points were 4.6 and 5.5, respectively. Therefore, their shifts in isoelectric points were lower than those for the isotropically modified materials and, contrary to the latter, they changed with the size of the silica nanoparticles. Hence, a shorter shift in isoelectric point was recorded for the larger silica nanoparticles. This suggests that the coverage of the surface of the nanoparticles functionalized anisotropically with APTES increased when decreasing the particle size of silica. Similar behavior has been reported by Zenerino et al.[59] for SiO_2 Janus nanoparticles functionalized with APTES.

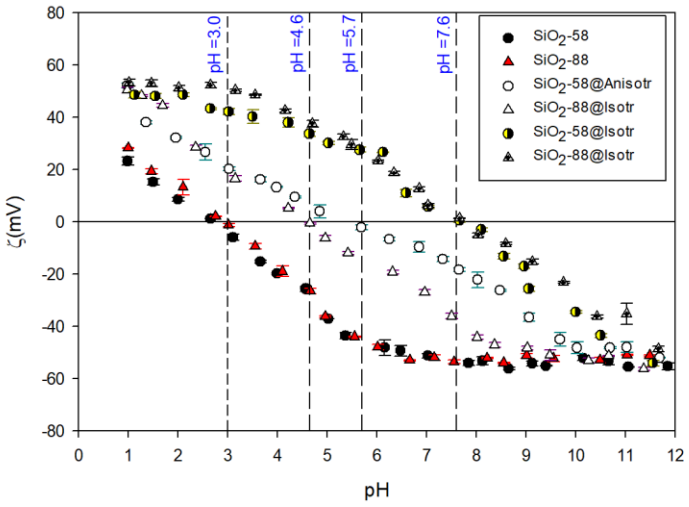

Figure 3. Z potential profile over the pH of the different materials. The horizontal line denotes $\zeta = 0$ mV, and the vertical lines represent some fixed pH values. All experiments were performed by triplicate, and the showed values are the respective mean with the standard deviation.

Static contact angle measurements between samples of the particles and of a drop of water in an air atmosphere were done. The results are shown in **Table 1** and some images are reported in **Figure S6**. SiO_2 materials were the most hydrophilic among the studied materials, contact angle ~ 48°, while the functionalized materials became less hydrophilic, contact angle ≥ 53°. The materials functionalized by the isotropic method were the least hydrophilic, contact angle for SiO_2-58@Isotr and SiO_2-88@Isotr ~ 55°. The observed increase of contact angle was somehow expected because the carbon backbone of APTES replaces the surface -OH groups of the silica during functionalization. On the other hand, the particle size of silica did not seem to significantly affect the contact angle of the functionalized materials.

Thermogravimetric analysis has proven to be an adequate tool for assessing the quantity of APTES chemisorbed on functionalized silica particles.[60] **Figure 4** shows the thermogravimetric profiles for samples of SiO_2-58, SiO_2-58@Anisotr, and SiO_2-58@Isotr.

Sample	Particle diameter (nm)	IEP	Contact angle (°)	%W_{APTES}	APTES/OH
SiO_2-58	58±4*, 60±4$^{\infty}$	2.7	47.9±0.3	0.0	N.A.
SiO_2-58@Anisotr	62±3$^{\infty}$	5.7	53.0±0.5	5.5	0.9
SiO_2-58@Isotr	63±3$^{\infty}$	7.8	55.8±0.3	9.8	1.6
SiO_2-88	88±5*, 89±3$^{\infty}$	2.7	48.1±0.5	0.0	N.A.
SiO_2-88@ Anisotr	92±5$^{\infty}$	4.6	53.2±0.2	4.6	0.8
SiO_2-88@ Isotr	91±5$^{\infty}$	7.8	55.4±0.3	9.5	1.7

Table 1. Samples properties obtained from several techniques. **Particle diameter**: Obtained from a statistical analysis of the SEM micrographs* or by DLS$^{\infty}$. **Isoelectric point (IEP):** Determinate by zeta potential over a pH range **Contact angle (°):** measured by the static contact angle between water and the corresponding nanomaterial in an air environment at 25°C. **% W_{APTES}**: Determinate by TGA data through a mass balance represented in eq. 1. consideration. **APTES/OH**: Experimental APTES/OH surface ratio calculated with TGA data and Zhuravlev[61] α_{OH} value.

The sample from SiO_2-58 lost 5.02 wt.% during the test. The recorded profile and the weight loss are typical for silica.[60] The ~0.98 wt.% loss from 100 to 190°C was due to the desorption of physisorbed water, while the weight loss from 190°C onwards is due to the dehydroxylation of surface silanols. For the sample from SiO_2-58@Anisotr, the wt.% loss due to desorption of water was ~0.93 wt.%, approximately the same as compared to SiO_2-58, while the wt.% loss at T > 190°C was higher hence being ascribed to the desorption of chemisorbed APTES. Considering that APTES boils at 217°C, the wt.% losses after such a temperature can be associated with its decomposition and further elimination from the material. In the literature, the desorption of chemisorbed APTES over silica nanoparticles was observed between 200 and 750°C.[60,62] Assuming that the weight loss due to dehydroxylation was negligible as compared to the APTES weight fraction, it was possible to estimate the weight percentage of chemically bonded APTES for each material doing a material balance, equation 2:

$$\%W_{APTES} = \left(\frac{m_{300} - m_{750}}{m_{300}}\right) x\ 100\% \qquad \textit{Equation 2.}$$

Where, m_T represents the residual weight of the sample at the T-th temperature of the TGA analysis. Table 2 shows the values obtained for this parameter.

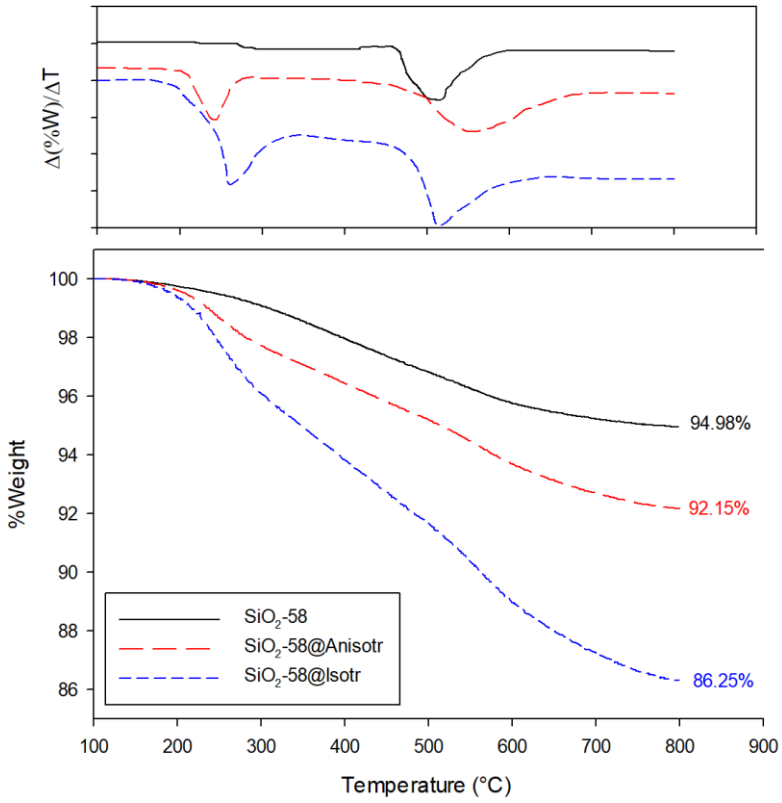

Figure 4. Thermogravimetric profiles for SiO_2-58 (continuum-black), SiO_2-58@Anisotr (dashed-red), and SiO_2-58@Isotr (dashed-blue). Top inset: first derivates of the featured TGA profiles.

According to Zhuravlev,[61] the concentration of -OH superficial groups is indistinct of the type of silica, with a value of $\alpha_{OH} \sim 5$ groups nm^{-2}. A rough estimation of the surface concentration -OH groups could be made taking into consideration the particles as perfect spheres (measuring their surface area and total volume) with diameters of 88 and 58 nm, the Avogadro number, and $\rho SiO_2 = 2.65$ g cm^{-3}. The values thus obtained were 2.1×10^{-4} and 3.2×10^{-4} mol OH g^{-1} SiO_2, for SiO_2-88 and SiO_2-58, respectively. Taking into consideration these values and the TGA results, an estimation of the APTES/OH ratio was done. These values (shown in Table 1) evidenced the differentiation in both kinds of particles when functionalized by the Pickering method or the conventional one, and they were in the range for the theoretical APTES/OH ratio[63] values from 0 to 3, forming mono-, bi-, and tridentate structures.[60] Moreover, the particles functionalized by the

Pickering method did not occupy all the available OH groups, which is in agreement with the DLS and contact angle results.

To summarize, non-porous spherical silica nanoparticles of two well-differentiated sizes were produced and functionalized with APTES by two methods; namely an isotropic and an anisotropic method. Regardless of the size of the silica nanoparticles, the isotropic method produced functionalized nanoparticles with a higher degree of functionalization which hence led to a higher isoelectric point and a higher degree of hydrophobicity. The collected evidence allows to conclude that the silica nanoparticles functionalized by the anisotropic method are Janus nanoparticles. In what follows, the characteristics of emulsions formulated with these nanoparticles are investigated.

Formulation of emulsions using isotropically functionalized silica nanoparticles. Figure S7 shows a photograph of a squalene-water emulsion formulated with SiO_2-58@Isotr. In general, the emulsion broke in 10 min upon its formation. This behavior was ascribed to the fact that the functionalizing agent completely covered the surface of these silica nanoparticles. Therefore, they would not interact with the water phase of the system which results in a rapid coalescence of the droplets. Considering these results, isotropically functionalized nanoparticles were no longer considered for analysis.

Formulation of emulsions using Janus silica nanoparticles. Figure 5 shows pictures of the emulsions formulated with the Janus silica nanoparticles and with vacuum gas oil (orange) and squalane (white). These emulsions were stable for more than 24 h. Their nature changed with the type of oil phase. When the oil phase was squalane, the emulsions were of the oil in water type, whereas the emulsions were of the water in oil type when the oil phase was the vacuum gas oil. Proof of this conclusion was that the conductivity of the squalane/Janus silica/water emulsions was between 3.3 – 4.5 $\mu S\ cm^{-1}$, while the conductivity of the water/Janus silica/vacuum gas oil system

was 0.1 – 0.3 μS cm^{-1}; i.e., the conductivity of the squalane/Janus silica/water emulsions approached the value of conductivity of the oil phase while the conductivity of the water/Janus silica/vacuum gas oil system approached the value of conductivity of water.[64] Further proof of the change in the nature of the formulated emulsions with the change in the used oil phase was provided by the results of the drop dissolution tests shown in **Figure S8**. Therefore, the formulated Janus silica nanoparticles produced both oil in water and water in oil emulsions depending on the nature of the oil phase. Typically, oil in water emulsions are stabilized by hydrophilic particles and viceversa; i.e. water in oil emulsions are stabilized by hydrophobic particles.[15,65] Therefore, the formation of the squalane/Janus silica/water emulsions was expected while formation of the water/Janus silica/vacuum gas oil emulsions was not. Next, a separate analysis of the characteristics of these two types of emulsions is presented.

Figure 5. Photographs of vacuum gas oil-water (orange) and squalane-water (white) emulsions formulated with SiO_2-58@Anisotr (left side of the pictures) and SiO_2-88@Anisotr (right side of the pictures). The formed emulsions were stable for a period longer than 1 day upon their formation.

Characteristics of the squalane/Janus silica/water emulsions. According to the measured droplet size distributions, **Figure S9** and **Table S2**, the emulsions produced with the Janus silica nanoparticles had monomodal droplet size distributions and average droplet diameters ranging

from ~0.45 μm to ~1.60 μm.[66] A statistical analysis of the effects of the factors involved in the formulation of these emulsions over their average droplet diameters ($D_{50\%}$) and over the polydispersity of their droplet size distributions will now be made. The raw data for these two metrics are reported in **Tables S2** and **S3**, respectively.

Figures 6 and **7** present a series of statistical plots for analyzing the effect of the factors of the designed 2^3 experiment over the square root of the $D_{50\%}$ average droplet diameter of the squalane/Janus silica/water emulsions. The square root transformation of the $D_{50\%}$ raw data was necessary to stabilize the variance of the residuals of the ANOVA model. This kind of transformation is well explained in statistical textbooks.[67,68] A scaling of the response variable does not imply any wrongs during experimentation but helps making an adequate statistical assessement of the effects of the factors investigated in the experiment.[69] **Figure 6** shows main effects and interaction plots for detecting and cataloging the effects of the factors of the experiment over the square root of the average droplet size of the formulated emulsions. Meanwhile, **Figure 7** shows the corresponding analysis of variance table plus the analysis of the residuals of the ANOVA model. The latter must observe a linear pattern for the normality test and random patterns for the constant variance tests in order to warrant the reliability of the ANOVA.[67,68,70] The effects of the factors involved in the experimental design were classified as positive when the response variable increased with the increase of the corresponding main factor and as negative when the response variable decreased with the increase in the corresponding main factor. Regarding the interaction factors, these were classified as synergistic when the slopes of the curves plotted for each level of the factor plotted as secondary (the levels of the factor plotted as primary are represented in the x-axis of the plot) have the same sign. The denominations primary and secondary serve merely as guidance for making interaction plots. Overall, we followed the principles stated

by Wu & Hamada[67], Quinn and Keough,[70] and Wagenmakers et al.[71] for making the presented plots and interpreting them.

According to the statistical analysis, the effects of the main factors of the experiments followed the order, **Figure 7**: d_p > ε >> W%, where, both the effects of the average particle size of the silica nanoparticles and the energy of emulsification were negative and statistically significant at a 95% significance level. Meanwhile, the effect of the water percentage of the emulsions was positive but not strong enough as to be considered statistically significant. Considering these tendencies, one may conclude that the emulsions formulated with both the largest silica nanoparticles and the highest emulsification energy had the smallest droplets regardless of the water percentage. On the other hand, the effect of the second order interaction factors followed the order: d_p×ε ≥ W%×ε >> W%×d_p. According to the ANOVA test, the W%×d_p interaction was not statistically significant at the 95% confidence level. Therefore, only the d_p×ε and W%×ε interactions will be analysed further. In this regard, both the interaction plots for the d_p×ε interaction, **Figure 6**, showed a synergistic behavior, meaning that the behavior of the response variable always followed the same trend regardless of the levels set for these two input variables. However, the statistical interpretation of this interaction is difficult because the plotted curves did not cross hence being considered a borderline interaction, i.e., one that may or may not be removed from the ANOVA model.[71] In the case of the present data, this interaction corresponded to the two main factors who had the stronger effects over the response variable. Therefore, it is possible that the d_p×ε interaction is a consequence of the latter and not due to the non-additivity of the effects of these two factors. Such a conclusion is supported by the fact that the slope of the curves for both the low levels of d_p and ε approched zero for both the d_p×ε and the ε×d_p reciprocal plots, **Figure 6**. Further support for this interpretation is provided by the hierarchy

principle in experimental design[67] which states that lower-order effects are more likely to be important than higher order effects.[67] On the other hand, the plots for the W%×ε interaction, **Figure 6**, showed a cross, W%×ε –synergistic–, and two converging lines ε×W% –antagonistic–. This kind of behavior indicates that the interaction between the water content of the emulsion and the emulsification energy is not removable by a monotonic change of the measurement scale which implies that this is a non-additive effect that must be considered when modeling the dependence of the square root of the average droplet size over these two variables. Such a conclusion is further supported by the ANOVA test which showed statistical significance at the 95% confidence level for this factor, **Figure 7**. Finally, the statistical analysis of the data revealed that the triple interaction of the input variables of the experiment can be ruled out since two, ε×W%×d_p and d_p×ε×W%, of the triple interaction plots, **Figure 6**, were almost parallel and the other one, W%×d_p× ε, did not cross. Meanwhile, the ANOVA test showed that this factor did not surpass the 95% confidence limit for statistical significance, *p-value* ≈ 0.5809.

To summarize, one may say the following about the above results: (i) the average diameter of the silica nanoparticles and the emulsification energy had the strongest effects over the average droplet size of the squalane/Janus silica/water emulsions. The effect consists of a decrease of the average droplet size of the emulsions when increasing both the average diameter of the silica nanoparticles and the energy applied during emulsification. This is in alignment with previous reports in which the particles sizes and applied energy are inversely proportional to the droptlet size.[72–74] (ii) There was no evidence indicating that the water content of the emulsions had an effect over the average droplet size of the formulated emulsions. (iii) There was evidence of the existence of non-additive effects between the water content and the emulsification energy and between the average diameter of the silica nanoparticles and the emulsification energy.

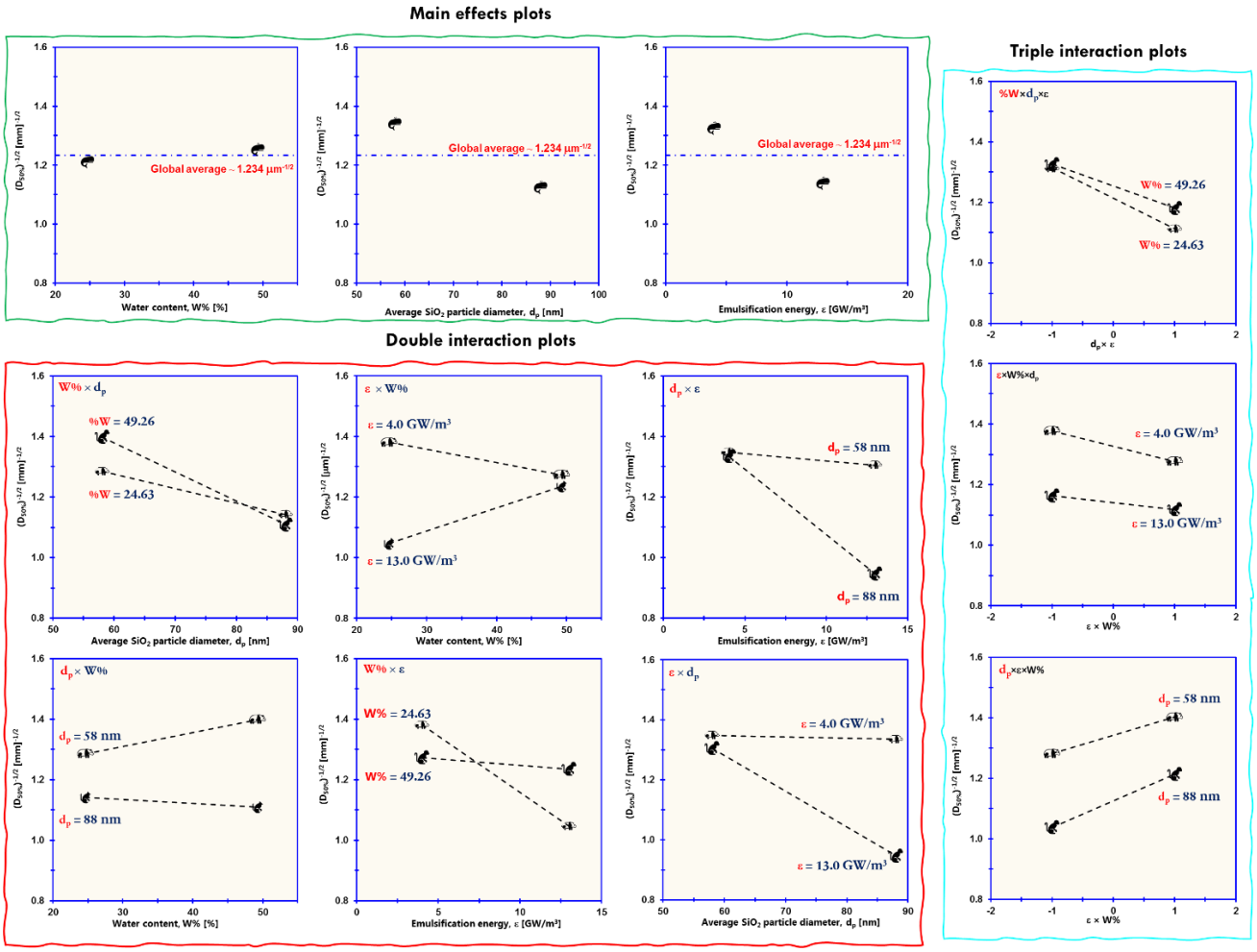

Figure 6. Plots for detecting the effects of the main factors, particle size of the silica nanoparticles -d_p-, water content, W%, and emulsification energy, ε, of the interaction factors, d_p×W%, d_p×ε, W%×ε, and d_p×W%×ε of the 2^3 experiment over the square root of the average, $D_{50\%}$, droplet size of the squalane/Janus silica/water emulsions.

Analysis of Variance table

Factor	Effects	Type of effect	SS	%Contr to SS	υ	MS	F ratio	*p-value*	*Sign* (95%)*
W%	0.0406	Very weak, positive	0.00658	1.0325	1	0.0066	0.70	0.4255	No
d_p	**-0.2159**	**Strong, negative**	0.18649	29.2665	1	0.1865	19.98	0.0021	**Yes**
ε	**-0.1861**	**Strong, negative**	0.13847	21.7317	1	0.1385	14.84	0.0049	**Yes**
W%×d_p	-0.0730	Weak, W%×d_p = synergistic; d_p×W% = antagonistic	0.02131	3.3449	1	0.0213	2.28	0.1692	No
W%×ε	**0.1476**	**Strong, W%×ε = synergistic; ε ×W% = antagonistic**	0.08714	13.6749	1	0.0871	9.34	0.0157	**Yes**
d_p×ε	**-0.1728**	**Strong, d_p×ε = synergistic; ε ×d_p = synergistic**	0.11946	18.7484	1	0.1195	12.80	0.0072	**Yes**
W%×d_p×ε	0.0278	Very weak, synergistic	0.00309	0.4848	1	0.0031	0.33	0.5809	No
Error			0.0747		8	0.0093			
Total			0.6372		15				

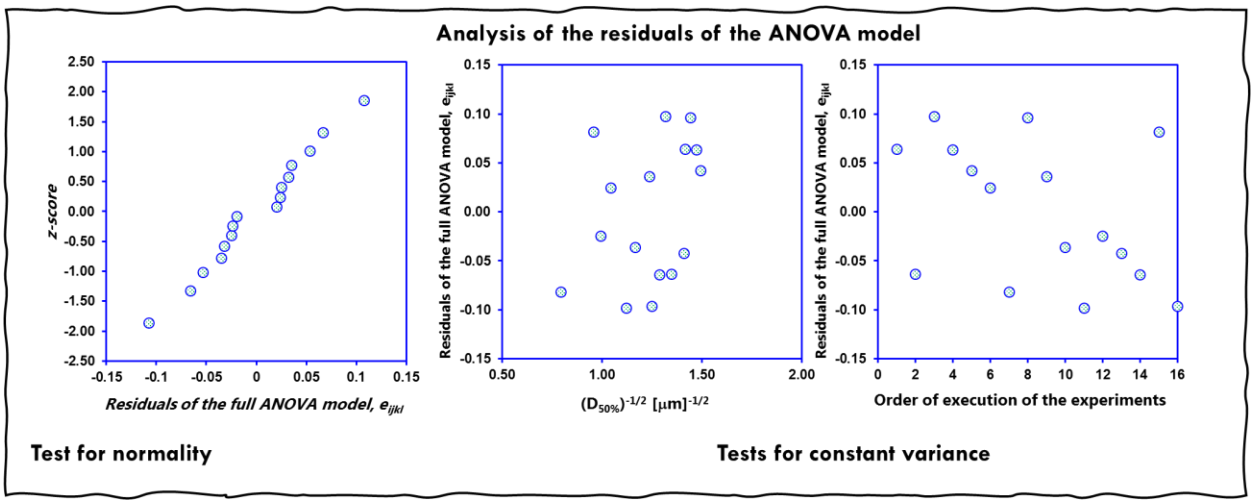

Figure 7. Analysis of variance for assessing the effects of the main factors, particle size of the silica nanoparticles -d_p-, water content, W%, and emulsification energy, ε, of the interaction factors, d_p×W%, d_p×ε, W%×ε, and d_p×W%×ε of the 2^3 experiment over the square root of the average, $D_{50\%}$, droplet size of the squalane/Janus silica/water emulsions. *Sign = significance level.

Polydispersity ranged between ~0.42 and ~0.91, which shows that the emulsions had a very heterogeneous distribution of size populations. The individual detection of these populations may have escaped detection by DLS.[75] Therefore, it should be admitted that the interpretation of the present data has a rather qualitative value.

Figure 8 shows the ANOVA table and the corresponding residuals of the ANOVA model used for the statistical assessment of the effects of the factors of the designed experiment over polydispersity. Main effects and interaction plots are presented in **Figure S10**. In this case, the only factor that showed a strong, positive, and statistically significant effect over polydispersity was the water content of the emulsion. Therefore, none of the factors that modified the average droplet size distribution of the emulsions had an effect over polydispersity.

Analysis of Variance table

Factor	Effects	Type of effect	SS	%Contr to SS	υ	MS	F	p-value	Sign*(95%)
W%	**0.1938**	**Strong, positive**	0.1502	48.9836	1	0.1502	14.75	0.0049	**Yes**
d_p	0.0513	Very weak, positive	0.0105	3.4273	1	0.0105	1.03	0.3394	No
ε	-0.0738	Very weak, negative	0.0218	7.0973	1	0.0218	2.14	0.1819	No
W%×d_p	0.0513	Weak, W%×d_p = synergistic; d_p×W% = antagonistic	0.0105	3.4273	1	0.0105	1.03	0.3394	No
W%×ε	-0.0488	Weak, W%×ε = synergistic; ε×W% = antagonistic	0.0095	3.1011	1	0.0095	0.93	0.3622	No
d_p×ε	0.0438	Weak, d_p×ε = synergistic; ε×d_p = antagonistic	0.0077	2.4976	1	0.0077	0.75	0.4111	No
W%×d_p×ε	-0.0612	Very weak, synergistic	0.0150	4.8953	1	0.0150	1.47	0.2593	No
Error			0.0815		**8**	0.0102			
Total			0.3065		**15**				

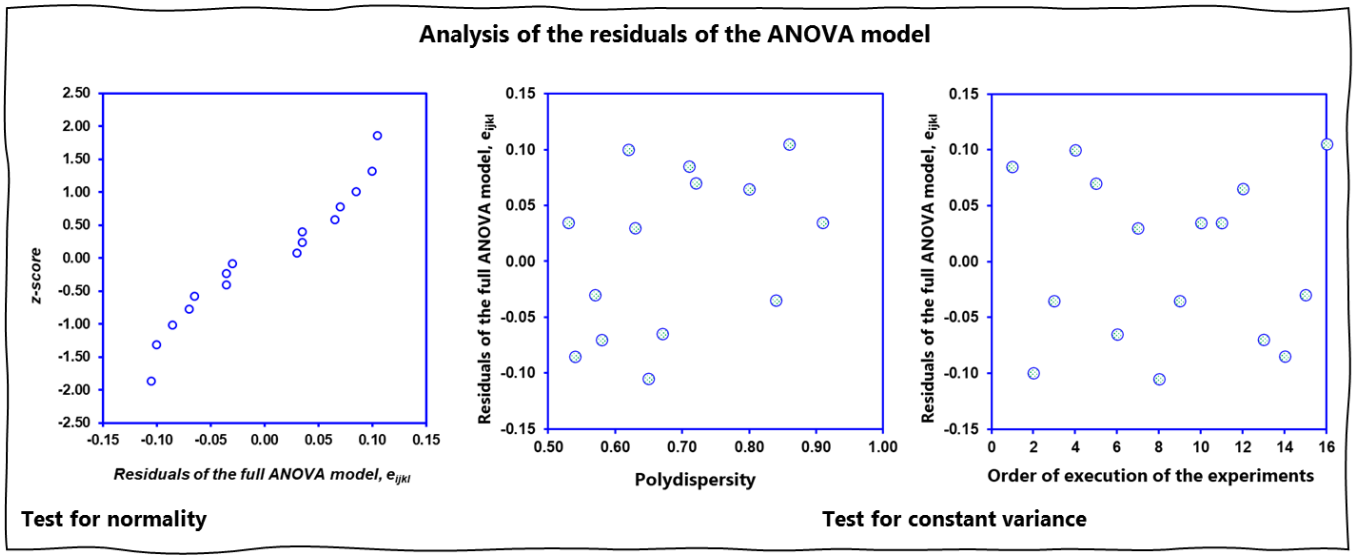

Figure 8. Plots for detecting the effects of the main factors, particle size of the silica nanoparticles -d_p-, water content, W%, and emulsification energy, ε, of the interaction factors, d_p×W%, d_p×ε, W%×ε, and d_p×W%×ε of the 2^3 experiment over the polydispersity of squalane/Janus silica/water emulsions.

Rheological behavior of the squalane/Janus silica/water emulsions. Flow curves for water, squalene, vacuum gas oil, squalane + Janus silica, and vacuum gas oil + Janus silica fluids are presented as references in **Figure S11** of the Supplementary Information. Its initial shear stress, τ_i, was 1×10^{-5} Pa with a corresponding viscosity, η, of 0.001 Pa.s all throughout the range of the tested shear rates: γ = 0.01 to 1000 s^{-1}. Squalane behaved as a Newtonian fluid with a viscosity of = 0.027±3.50×10-5 Pa·s,), which agreed with the value reported in the literature.[76]

The addition of Janus silica particles (1.48 wt.%) to squalene modified its rheological behavior, **Figure S11**. Shear thinning behavior was evidenced from the data for η. Namely, the system showed an onset viscosity, η_i, of ~0.184 Pa·s that decreased to η_∞ = 0.062 Pa·s. Notice that η_∞ for the squalane + Janus silica system was a little higher than η_∞ for squalane, which is a typical behavior for liquid fluids + nanoparticles systems.[15]

Figure 9 shows the flow curves for the emulsions formulated from the singly replicated 2^3 experiment considering the water percentage, average diameter of the silica nanoparticles, and the emulsification energy as input variables. In general, all the formulated emulsions showed shear thinning behavior.

In most cases, apparent yield stress, τ_0, was observed. The corresponding values for this parameter were tabulated in **Table S4**. A statistical analysis of the effects of the studied experimental factors over τ_0 is presented in **Figure 9** and **Table S5**. The only factor that had an effect over τ_0 was the content of water of the emulsions. **Figure 10** shows a main effect plot that allows establishing that the water content of the emulsions had a linear negative effect over τ_0. These results allowed concluding that increasing the loading of water in these emulsions increased their flowability.

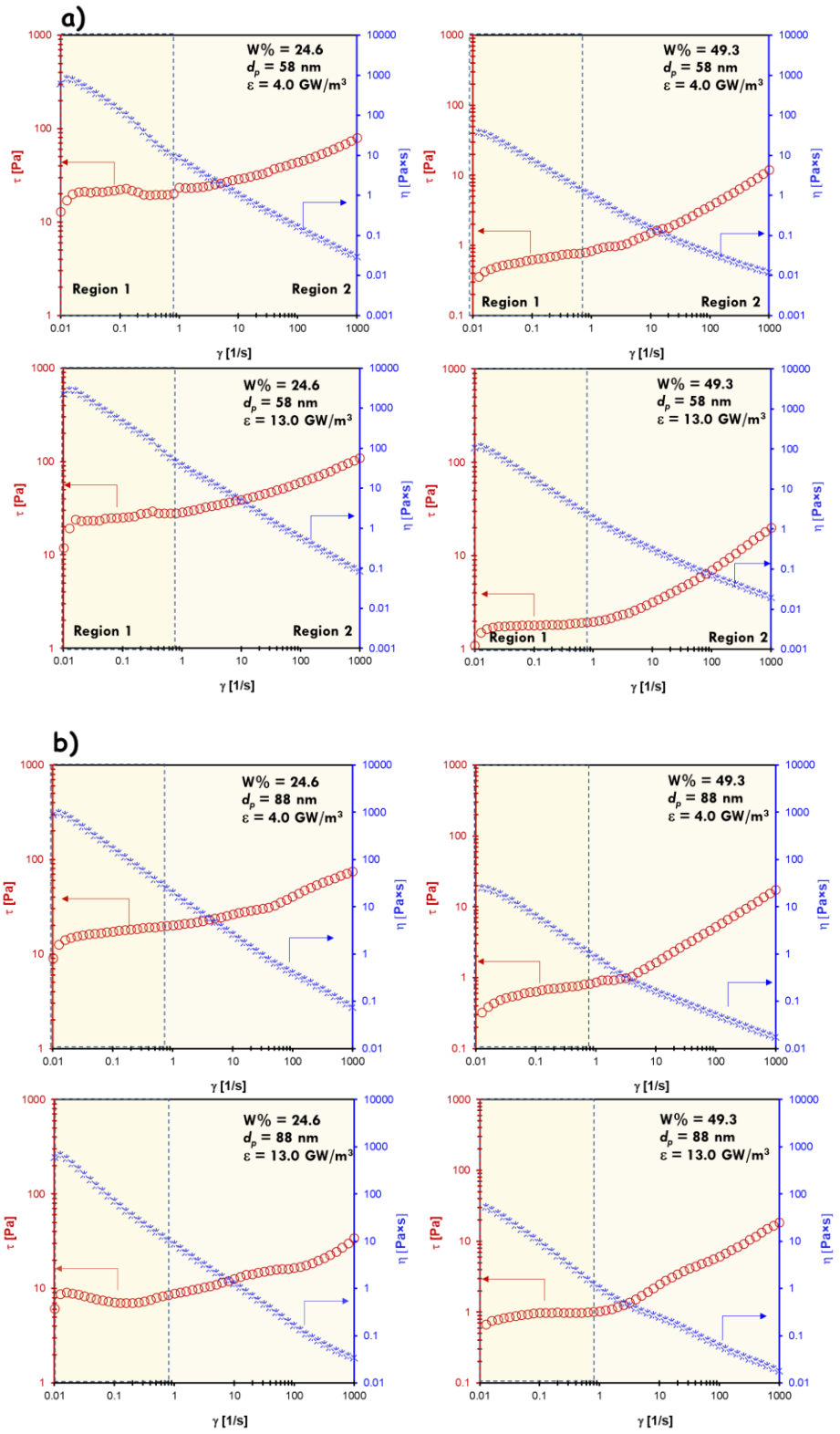

Figure 9. Flow curves for squalane/Janus silica/water emulsions formulated according to a single replicate 2^3 full factorial experiment considering the water content, W%, average size of the silica nanoparticles -d_p-, and emulsification energy, ε, as input variables.

For describing shear thinning, the data were fitted to the so-called power law model[77] starting from $\gamma \sim 1.00\ s^{-1}$. The power law model describes the rheology of a fluid in terms of two parameters; namely, the consistency index, K [=] $Pa \cdot s^n$, which is a descriptor of the effective viscosity of the fluid, and the flow behavior index, n, which measures the deviation of the behavior of the fluid as in regards to the Newtonian flow.

Figure 10 shows that an increase in the water content of the squalane/Janus silica/water emulsions decreased the consistency index in the same fashion as the value of τ_0. Meanwhile, the flow behavior index increased from $n < 1$, i.e., shear thinning behavior, to $n \sim 1.0$, i.e. Newtonian behavior, with the increase of the water content. It is noticeable that the other factors studied for the formulation of the emulsions had statistically negligible effects over the rheological parameters, **Tables S4 – S7**. Therefore, the increase in the content of water of these emulsions made them less viscous and more Newtonian as it was also evidenced by the flow curves shown in **Figure 11**. Indeed, the other two families of emulsions showed only shear thinning behavior with minimum viscosity similar to the viscosity of squalane, **Figure 11**.

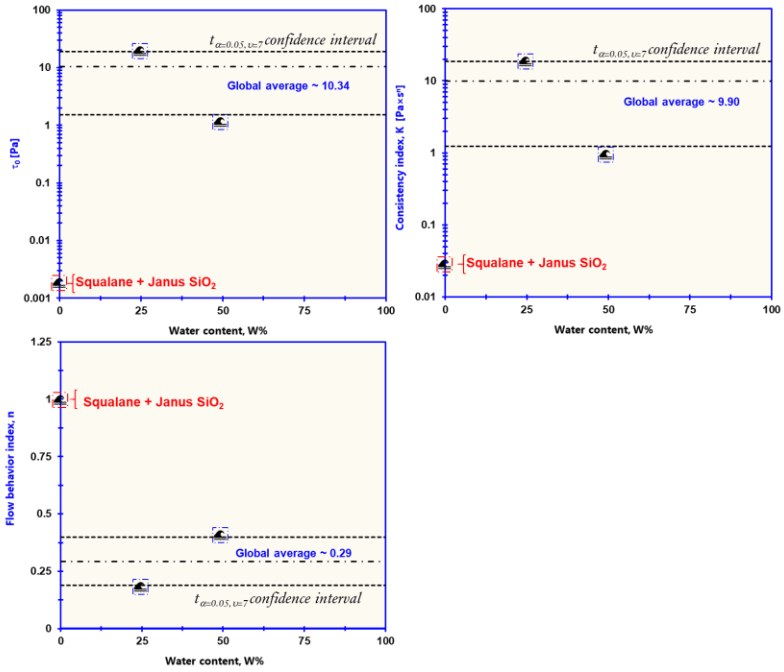

Figure 10. Main effect plots illustrating the effect of the content of water of the squalane/Janus silica/water emulsions over their rheological parameters: τ_0, consistency index, K, and flow behavior index, n.

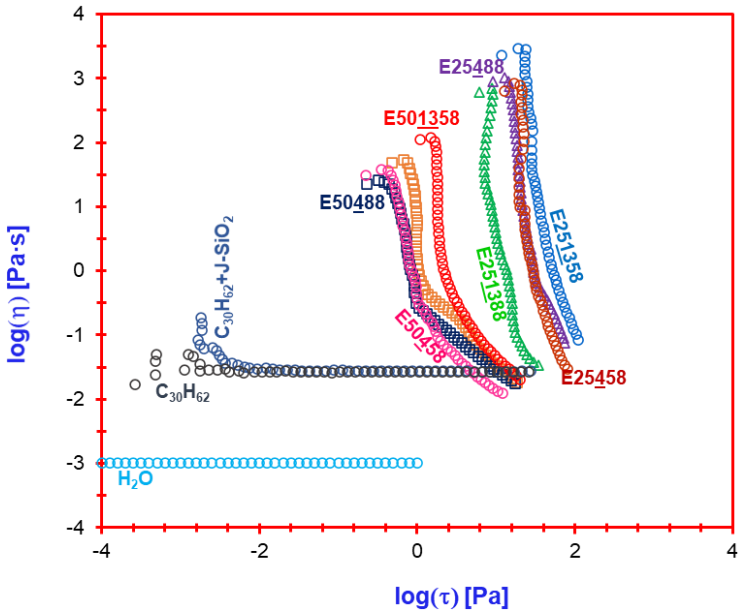

Figure 11. Flow curves for the squalane/Janus silica/water emulsions in terms of log(η) vs. log(τ). Nomenclature: E = emulsion; the first two digits of the code are the water percentage, the underlined digits are the emulsification energy, and the last two digits are the average diameter of the silica nanoparticles. $C_{30}H_{62}$ = squalane. J = Janus.

Figure 12a plots η_i -a descriptor of the viscosity of the emulsions at the lowest applied shear rate- as a function of the average diameter of the droplets for each one of the formulated squalane/Janus silica/water emulsions. There was a saddle-shape correlation for the data with a minimum initial viscosity for the emulsion formulated with 50% water, Janus silica nanoparticles of average diameter equal to 58 nm, and using an emulsification energy of 4.0 GW/m^3. The shape of the observed correlation curve for the data set reflects the existence of the non-additive effects between the factors influencing the droplet size distributions of the emulsions discussed earlier, **Figure 7**. Typically, the literature considers that the viscosity of an emulsion increases with the decrease in the size of its droplets when all the other factors are kept constant.[66,78,79] However, the behavior of the current coarse emulsions was more complicated than that. On the other hand, a linear correlation between the polydispersity of the droplet size distributions was found, **Figure 12b**. It can be recalled that, contrary to the behavior of the average droplet size distribution, the polydispersity of the squalane/Janus silica/water emulsions was only influenced by the content of water of the emulsions. The literature postulates[66,79] that a decrease in polydispersity is expected to decrease the viscosity. As observed, this was not the case for the current emulsions. Therefore, in general, the behavior of the squalane/Janus silica/water emulsions cannot be completely explained by principles found for emulsions whose behavior has been studied with the classical one factor at a time experimental approach.

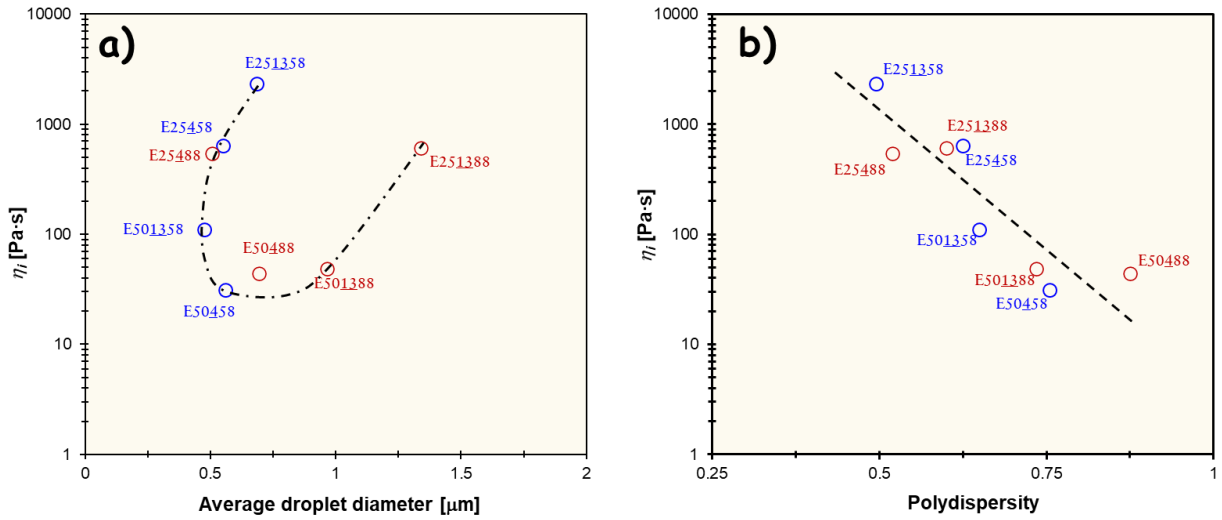

Figure 12. Plots of η_i vs. (a) average droplet diameters and (b) polydispersity. Nomenclature: E = emulsion; the first two digits of the code are the water percentage, the underlined digits are the emulsification energy, and the last two digits are the average diameter of the silica nanoparticles.

Characteristics of the water/Janus silica/vacuum gas oil emulsions.

The API gravity and chemical composition of the vacuum gas oil studied herein were reported in a previous work.[80] This vacuum gas oil corresponded to a heavy oil with total sulfur and nitrogen contents of ~1.04 and ~0.143 wt.%, respectively. In addition, the vacuum gas oil also contained ~3.11 wt.% resins and acidic oxygenated structures. Accordingly, it could be expected that the properties of the water/Janus silica/vacuum gas oil emulsions differed from those found for the squalane/Janus silica/water emulsions. Indeed, it was already commented that the former were water in oil and the latter oil in water.

The measured droplet size distributions for these emulsions and the average droplet sizes are presented in **Figure S12** and **Table S8**, respectively. Results showed that coarse water in oil macroemulsions with monomodal droplet size distributions and average droplet diameters ranging from ~0.40 μm to ~1.44 μm were produced. The statistical analysis of the average droplet

diameters ($D_{50\%}$) and the polydispersity of their droplet size distributions data is presented next. Raw data are shown in **Tables S8** and **S9,** respectively

The statistical analysis of the effects of the factors studied for the formulation of the water/Janus silica/vacuum gas oil emulsions over their average $D_{50\%}$ droplet size is presented in **Figures 13** and **S13**. Except for the second order W%×ε interaction, all the studied factors of the experiment had strong effects over the average droplet diameter of the emulsions. Also, all the main factors of the experiment had strong negative effects whose strength followed the order: ε (*p-value* $\approx 4.63\times10^{-5}$) > d_p (*p-value* ≈ 0.0072) ≥ W% (*p-value* ≈ 0.0045). Considering the statistically significant non-additive factors –W%×d_p, d_p×ε, and W%×d_p×ε–, these were all synergistic and strong. These trends differed from what was observed for the oil in water squalane/Janus silica/water emulsions (Figures **6** and **7**). These differences are related to the fact that the water percentage of the latter had a weak but positive effect over their behavior. Overall, the results of the statistical analysis suggested that controlling the average droplet size of the water/Janus silica/vacuum gas oil emulsions requires considering strong second and triple order non-additive effects into account.

Analysis of Variance table

Factor	Effects	Type of effect	SS	%Contr to SS	υ	MS	F	p-value	Sign*(95%)
W%	0.1655	**Strong, positive**	0.1096	4.9645	1	0.0431	15.30	0.0045	**Yes**
d_p	-0.1515	**Strong, negative**	0.0918	4.1601	1	0.0176	12.82	0.0072	**Yes**
ε	-0.3358	**Strong, negative**	0.4509	20.4319	1	0.0003	62.97	4.63×10^{-5}	**Yes**
%W×d_p	-0.5128	**Strong, %W×d_p = synergistic; d_p×%W=synergistic**	1.0517	47.6527	1	0.0518	146.86	1.99×10^{-6}	**Yes**
%W×ε	0.0405	Very Weak, %W×P_{agit} = synergistic; P_{agit}×%W= antagonistic	0.0066	0.2973	1	0.0000	0.92	0.3665	No
d_p×ε	-0.1065	**Strong, d_p×ε = synergistic; ε×d_p = synergistic**	0.0454	2.0558	1	0.0018	6.34	0.0360	**Yes**
%W×d_p×ε	0.3138	**Strong, synergistic**	0.3938	17.8420	1	0.0003	54.99	7.51×10^{-5}	**Yes**
Error			0.0573		**8**	0.0027			
Total			2.2069		**15**				

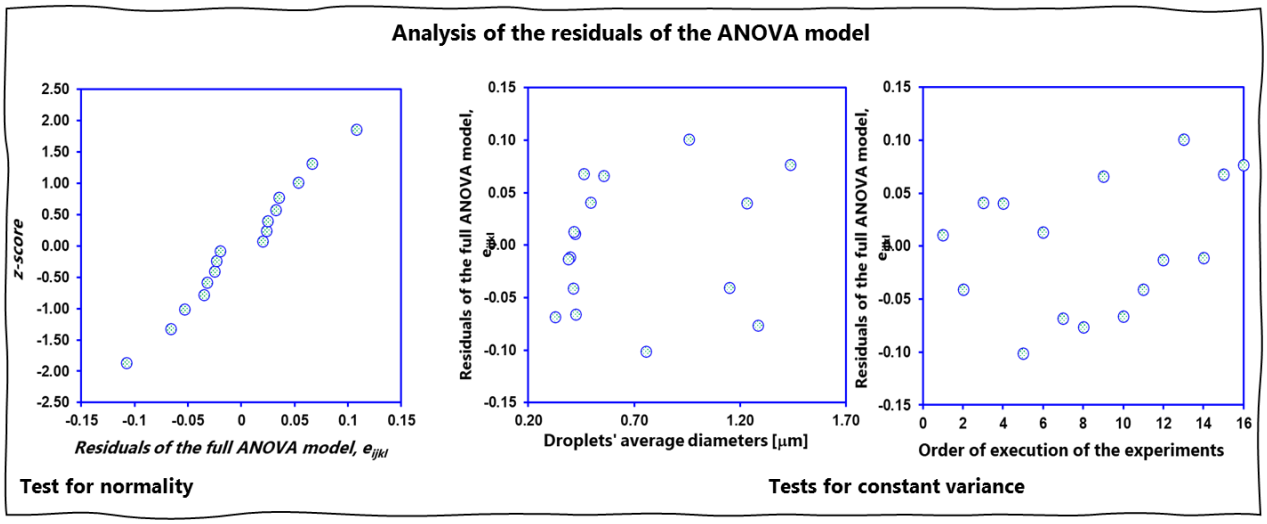

Figure 13. Analysis of variance for assessing the effects of the main factors, particle size of the silica nanoparticles -d_p-, water content, W%, and emulsification energy, ε, of the interaction factors, d_p×W%, d_p×ε, W%×ε, and d_p×W%×ε of the 2^3 experiment over the $D_{50\%}$ average of the droplet size of the water/Janus silica/vacuum gas oil emulsions. *Sign = significance level.

Figures 14 and **S14** show the statistical analysis of the effects of the studied experimental factors over the polydispersity of the droplet size distributions of the water/Janus silica/vacuum gas oil emulsions. Polydispersity was changed significantly by the water percentage, the particle size of the silica nanoparticles, and by the second order interaction between these two input variables, **Figure 14**. The strength of the effects of these factors followed the order: W% (*p-value* ≈ 0.0038) ≥ W%×d_p (*p-value* ≈ 0.0022) > d_p (*p-value* ≈ 0.0331). On the other hand, while the water percentage of the emulsions had a negative effect over the polydispersity, the average size of the silica nanoparticles had a positive effect. Meanwhile, the effect of the W%×d_p interaction was synergistic. In general, it can be noticed that polydispersity was most strongly influenced by the water content of coarse macroemulsions formulated with silica Janus nanoparticles regardless if they were of the oil in water or water in oil types.

Analysis of Variance table

Factor	Effects	Type of effect	SS	%Contr to SS	υ	MS	F	p-value	Sign*(95%)
W%	-0.1038	Strong, negative	0.0431	31.6488	1	0.0431	16.21	0.0038	Yes
d_p	0.0663	Strong, positive	0.0176	12.9049	1	0.0176	6.61	0.0331	Yes
ε	-0.0088	Very weak, negative	0.0003	0.2251	1	0.0003	0.12	0.7429	No
W%×d_p	-0.1138	Strong, %W×DE= synergistic; DE×%W=synergistic	0.0518	38.0438	1	0.0518	19.48	0.0022	Yes
W%×ε	0.0013	Very Weak, %W×P_{agit} = synergistic; P_{agit}×%W= antagonistic	0.0000	0.0046	1	0.0000	0.00	0.9625	No
d_p×ε	0.0213	Weak, DE×P_{agit} = synergistic; P_{agit}×DE = antagonistic	0.0018	1.3277	1	0.0018	0.68	0.4335	No
W%×d_p×ε	-0.0087	Very weak, synergistic	0.0003	0.2251	1	0.0003	0.12	0.7429	No
Error			0.0212		8	0.0027			
Total			0.1360		15				

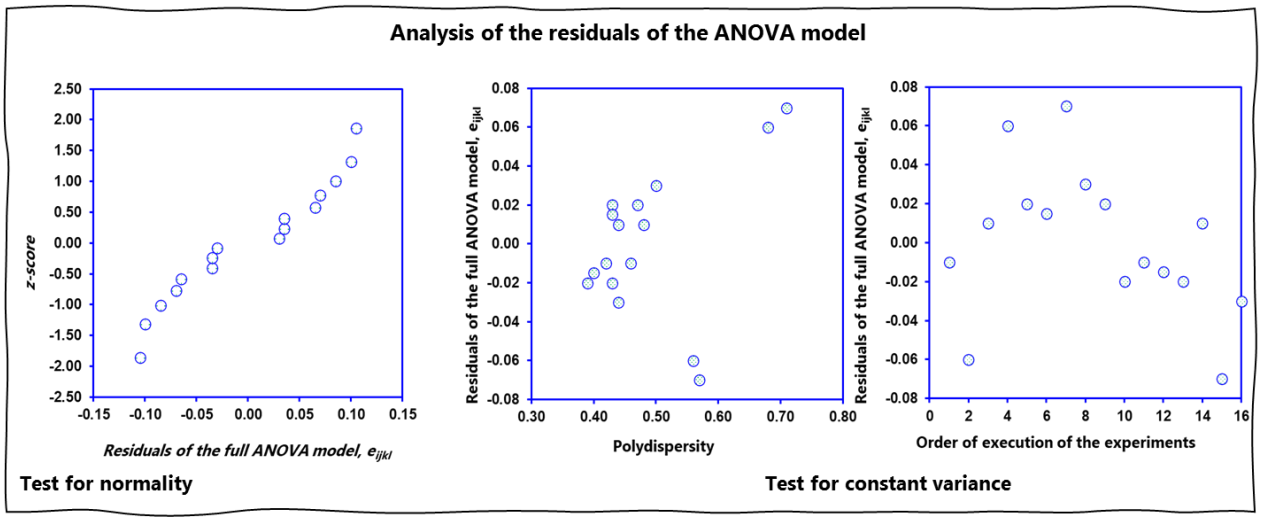

Figure 14. Analysis of variance for assessing the effects of the main factors, particle size of the silica nanoparticles -d_p-, water content, W%, and emulsification energy, ε, of the interaction factors, d_p×W%, d_p×ε, W%×ε, and d_p×W%×ε of the 2^3 experiment over the polidispersity of the droplet size distributions of the water/Janus silica/vacuum gas oil emulsions. *Sign = significance level.

Rheological behavior of the water/Janus silica/vacuum gas oil emulsions

Figure S11 shows the flow curves for the vacuum gas oil and the vacuum gas oil + Janus silica system. The vacuum gas oil showed a typical Newtonian behavior with a media $\eta = 2.946 \pm 3.00\times10^{-3}$ Pa.s (95% t-Student confidence interval with 50 degrees of freedom). This value agreed with the heavy oil character of the substance.[80,81] The addition of the Janus silica nanoparticles to the vacuum gas oil produced a Newtonian fluid with a higher viscosity, $\eta = 3.421 \pm 1.46\times10^{-2}$ Pa.s (95% t-Student confidence interval with 50 degrees of freedom) as compared to the vacuum gas

oil. This tendency suggested that the Janus silica nanoparticles interacted with the vacuum gas oil in a way that allowed the formation of a system whose structure emulated the one of a pure fluid.

Figure 15 shows the flow curves for the water/Janus silica/vacuum gas oil emulsions. In general terms, those emulsions with 25 % water content had a more Newtonian behavior than those of 50% as corroborated with flow behavior index, n **(Table S10)**. All of them exhibited shear thinning behavior with some of them exhibiting a certain degree of structure instability under certain shear rate conditions. Namely, the emulsion formulated with W% = 24.6, ε = 4.8 GW/m^3, and d_p = 58 nm, coded as E25558, as well as those coded as E25165 8, and E25588, displayed a sudden drop of viscosity for shear rates higher than 100 s^{-1}. In addition, the emulsion coded as E25168 8 showed structural transitions at lower shear rates. These changes can be ascribed to the deformation and further growth of the droplets of the emulsions during the rheological tests.[82]

To describe the rheological behavior of the emulsions, τ_{0i}, K, and n were estimated from the flow curves shown in **Figure 15**. In this case, τ_{0i} was taken as the value of shear stress recorded for the lowest shear rate of each experiment. On the other hand, K and n were the power law parameters for the fitting of the flow curves between γ = 0.01 and 100.00 s^{-1}. The latter procedure was adopted because of the already commented instabilities of the recorded flow curves at higher shear rates. **Table S10** shows the values of these parameters for each one of the formulated emulsions.

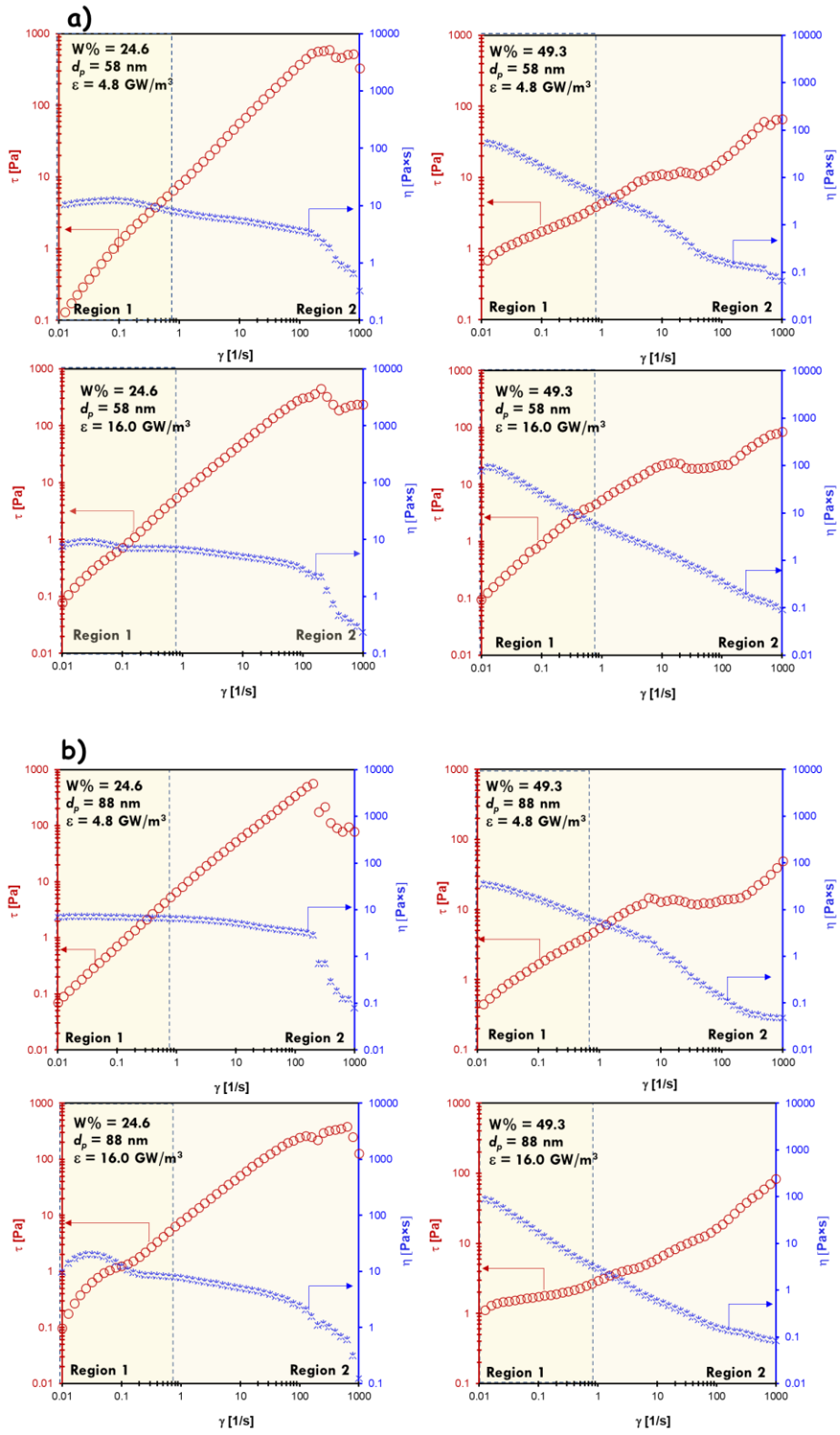

Figure 15. Flow curves for water/Janus silica/vacuum gas oil emulsions formulated according to a 2^3 full factorial experiment considering the water content, W%, average size of the silica nanoparticles -d_p-, and emulsification energy, ε, as input variables.

The statistical analysis of the data, **Figure 16** and **Tables S11 – S13**, led to conclude that only the water content of the emulsions may have had an effect over τ_{0i} and K. However, a definite conclusion on the observed effects could not be reached since there was not a complete correspondence between the analysis made with the main effect plots, **Figure 16**, and the results of the ANOVA tests, **Table S11 – S12**, because the *p-values* for this factor were larger than the 95% confidence limit. However, the test captured the fact that the water content was the factor that most influenced the variance of the experiment, see %contribution to the sums of squares in **Tables S11** and **S12**. Anyway, while the tendency showed by τ_{0i} as a function of the water content, volcano plot, is hard to explain, the tendency displayed by K was coherent with the fact that more diluted water in oil emulsions should display lower viscosity.

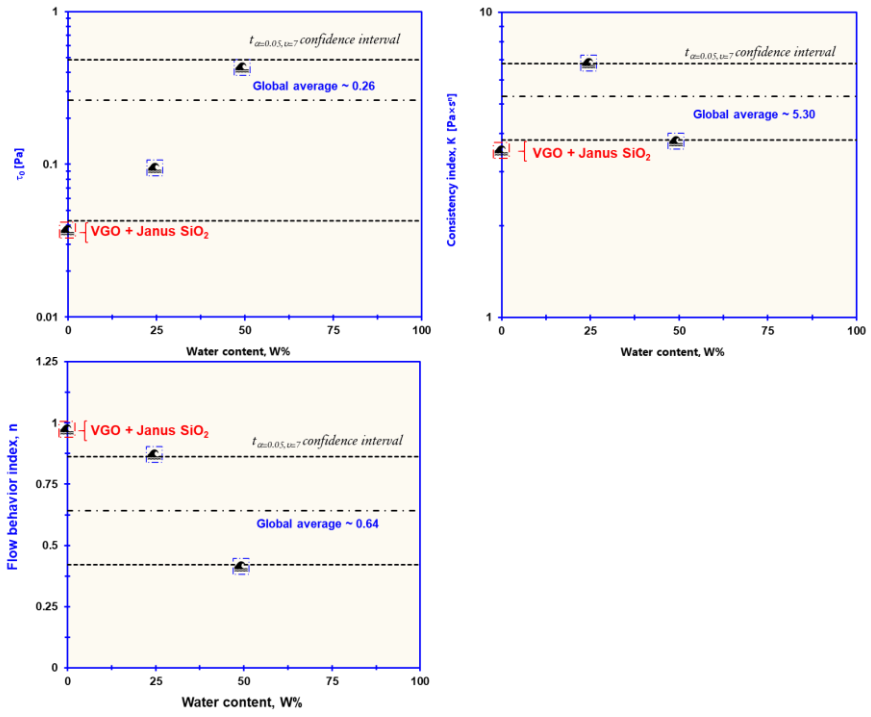

Figure 16. Main effect plots illustrating the effect of the content of water of the water/Janus silica/vacuum gas oil emulsions over their rheological parameters: τ_0, consistency index, K, and flow behavior index, n.

The flow behavior index displayed an inverted volcano plot type tendency with the content of water. In this case, the ANOVA test, **Table S13**, was also able to detect that the average size of the silica nanoparticles and the $d_p \times \varepsilon$ factor had effects whose *p-values* were lower than the 95% confidence threshold. Considering the ensemble of these analyses, one may conclude that an understanding the rheological behavior of the water/Janus silica/vacuum gas oil emulsions must consider the influence of non-additive factors involved in their formulation. The volcano plots found in **Figure 16** attest the influence of such effects. On the other hand, the flow curves presented in **Figure 17** show how some of the formulated emulsions approached a Newtonian behavior with viscosities very near the one of the vacuum gas oil phase, while others had a net shear thinning character with their viscosity decreasing to an intermediate value between the viscosity of water and vacuum gas oil.

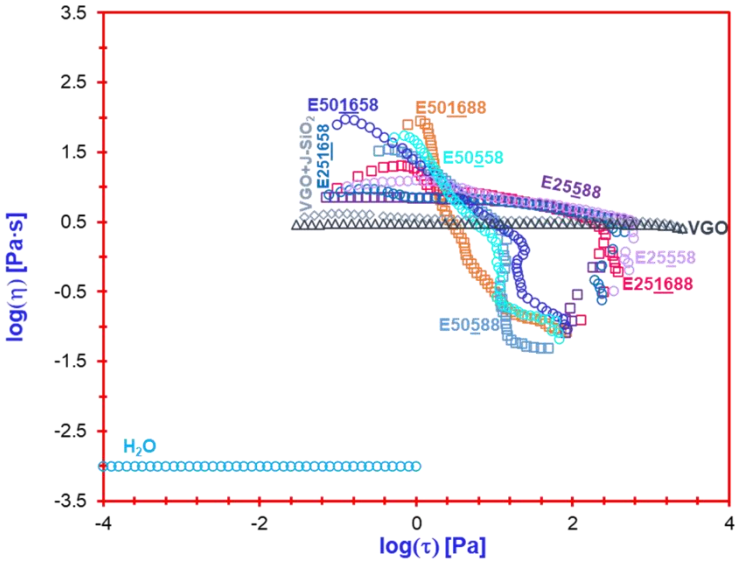

Figure 17. Flow curves for the water/Janus silica/vacuum gas oil emulsions in terms of log(η) vs. log(τ). Nomenclature: E = emulsion; the first two digits of the code are the water percentage, the underlined digits are the emulsification energy, and the last two digits are the average diameter of the silica nanoparticles. VGO = vacuum gas oil, J = Janus.

Finally, **Figure 18** shows that the viscosity of the water/Janus silica/vacuum gas oil emulsions have a non-linear correlation with their average droplet size, **Figure 18a**, and a roughly linear correlation with polydispersity, **Figure 18b**. These tendencies were similar to the ones found for the squalane/Janus silica/water emulsions. But, in this case, the curve found for the η_i vs. average droplet diameter plot displayed two regions with roughly constant viscosity preceded by viscosities with a ca. one order of magnitude gap.

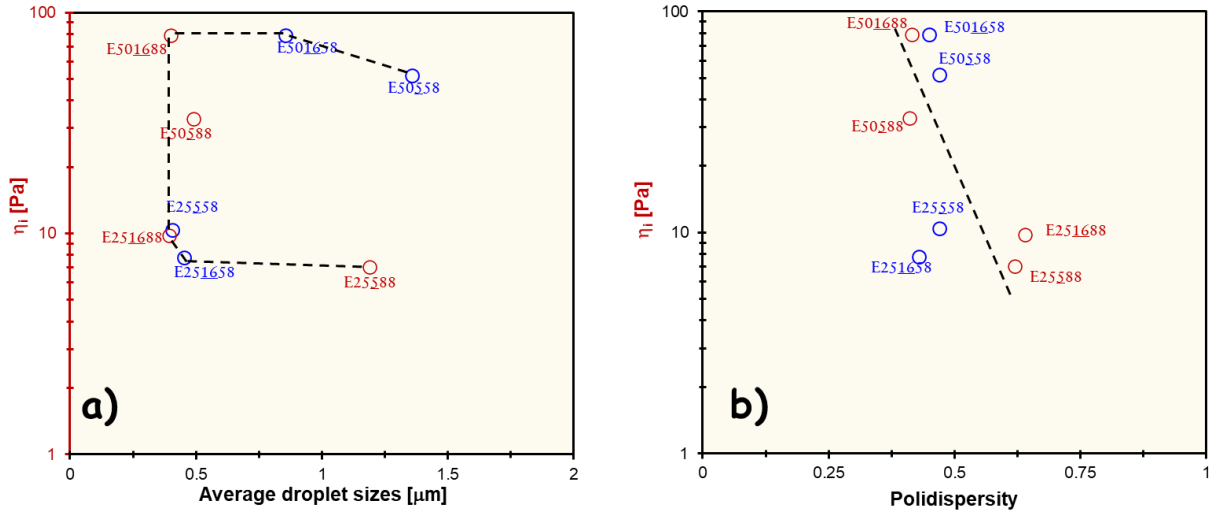

Figure 18. Plots of η_i vs. (a) average droplet diameter and (b) polydispersity. Nomenclature: E = emulsion; the first two digits of the code are the water percentage, the underlined digits are the emulsification energy, and the last two digits are the average diameter of the silica nanoparticles.

3. CONCLUSIONS

In this contribution, SiO_2 Janus nanoparticles of two different sizes were synthesized and used as surfactants for formulating macroemulsions composed of water and two different oil phases: squalane and vacuum gas oil. The influence of the particle size, the water content, the emulsification energy, and of the second and third order interactions between these variables over the droplet size distributions, polydispersity, and rheological profiles of the emulsions was investigated. The following conclusions were reached from the results of the study: (i) the nature

of the emulsions formulated with the synthesized SiO_2 Janus nanoparticles depended on the chemistry of the oil phase; namely, squalane formed squalane/Janus SiO_2/water (i.e., oil in water) emulsions while vacuum gas oil formed water/Janus SiO_2/vacuum gas oil (i.e., water in oil) emulsions; (ii) for the formulated oil in water emulsions, the droplet size distributions was modified by the particle size of the SiO_2 Janus nanoparticles, the emulsification energy and their interaction while the other experimental factors had no effect. Meanwhile, the polydispersity was only changed by the water content of the emulsions. On the other hand, these emulsions exhibited shear thinning behavior which was strongly dependent on the water content and not on the other experimental factors. (iii) for the water in oil emulsions, the average droplet diameter was influenced by all the experimental factors involved in their formulation except for the non-additive effect between the water content and the emulsification energy. Meanwhile, polydispersity was influenced by the particle size of the SiO_2 Janus nanoparticles, the water content and the interaction factor related to these two input variables. Accordingly, the rheological behavior of these emulsions was influenced by both the changes in the input variables and by the second interaction factors between these variables. Finally, regardless of the type of emulsion, an analysis of the rheological data and the average droplet diameter of these emulsions showed that these two parameters are non-linearly correlated. The ensemble of these results put into evidence that the formulation of emulsions using Janus nanoparticles requires the consideration of non-additive effects when aiming to achieve certain desirable characteristics for diverse applications in the oil industry.

AUTHOR INFORMATION

Corresponding Author

*Email: vicbaldo@uis.edu.co, Twitter: @vigabalme, Tel. +54 6344000 ext. 1485.

http://orcid.org/0000-0003-3227-0251.

ASSOCIATED CONTENT

The Supporting Information includes:

Experimental methods, SEM data, particle size measurements, N_2 physisorption isotherms, FTIR spectra, contact angle measurements, photographs of some emulsions, droplet size distributions, and statistical tests for the data.

Author Contributions

D.F.M., C.C.L-G & B.E.N-R work on the synthesis, purification, characterization and analysis of materials properties. C.C.L-G & B.E.N-R , and E.A-C in the preparation, characterization and reology of emulsions. D.F.M. revised and contributed to writing the manuscript. L.M.B.-R. directed and supervised the project as well as contributing and revising the writing of the manuscript. V.G.B.-M. supervised planned and was part of the execution of the project. He also revised and contributed to writing the manuscript. All authors have approved the final version of the manuscript

Notes

The authors declare no competing financial interest.

Funding Sources

This work was funded by Agencia Nacional de Hidrocarburos –ANH– and Minciencias, Colombia, within the frame of the Project 44842-365-2018: "*Preparación de nanomateriales*

basados en metales de transición para procesos ligados al recobro térmico de crudos colombianos y análisis de su comportamiento catalítico en procesos de combustión in-situ."

ACKNOWLEDGEMENTS

D.F.M., L.M.B.R., and V.G.B.M. are grateful for the financial support of Ministerio de Ciencia, Tecnología e Innovación (Minciencias) of Colombia, and the Agencia Nacional de Hidrocarburos (ANH) of Colombia through Project number FP44842-365-2018. E.A.C. thanks Minciencias for funding for his post-doctorate within the frame of the program "Es tiempo de Volver". Authors thank Laboratorio de Miscroscopía – UIS for SEM analysis.

4. REFERENCES

(1) Zhou, T.; Huang, Z.; Wan, F.; Sun, Y. Carbon Quantum Dots-Stabilized Pickering Emulsion to Prepare NIR Light-Responsive PLGA Drug Delivery System. *Mater. Today Commun.* **2020**, *23* (October 2019), 100951. https://doi.org/10.1016/j.mtcomm.2020.100951.

(2) Huma, S.; Khan, H. M. S.; Sohail, M.; Akhtar, N.; Rasool, F.; Majeed, F.; Daniyal, M. Development, in-Vitro Characterization and Assessment of Cosmetic Potential of Beta Vulgaris Extract Emulsion. *J. Herb. Med.* **2020**, *23* (August 2018), 100372. https://doi.org/10.1016/j.hermed.2020.100372.

(3) Yang, Y.; Fang, Z.; Chen, X.; Zhang, W.; Xie, Y.; Chen, Y.; Liu, Z.; Yuan, W. An Overview of Pickering Emulsions: Solid-Particle Materials, Classification, Morphology, and Applications. *Front. Pharmacol.* **2017**, *8* (MAY), 1–20. https://doi.org/10.3389/fphar.2017.00287.

(4) Peng, B.; Zhang, L.; Luo, J.; Wang, P.; Ding, B.; Zeng, M.; Cheng, Z. A Review of Nanomaterials for Nanofluid Enhanced Oil Recovery. *RSC Adv.* **2017**, *7* (51), 32246–32254. https://doi.org/10.1039/c7ra05592g.

(5) Prakash Sharma, V.; Sharma, U.; Chattopadhyay, M.; Shukla, V. N. Advance Applications of Nanomaterials: A Review. *Mater. Today Proc.* **2018**, *5* (2), 6376–6380. https://doi.org/10.1016/j.matpr.2017.12.248.

(6) Ruckenstein, E. Microemulsions, Macroemulsions, and the Bancroft Rule. *Langmuir* **1996**, *12* (26), 6351–6353. https://doi.org/10.1021/la960849m.

(7) Querol, N.; Barreneche, C.; Cabeza, L. F. Asphalt Emulsion Formulation: State of the Art of Formulation, Properties and Results of HIPR Emulsions. *Constr. Build. Mater.* **2019**, *212*, 19–26. https://doi.org/10.1016/j.conbuildmat.2019.03.301.

(8) Matsumoto, S. Preparation and State of Macroemulsions Stabilized by Small-Molecule Surfactants. *Top. Catal.* **1989**, *3* (4), 249–261. https://doi.org/10.1016/S0268-005X(89)80037-2.

(9) Zhu, Q.; Pan, Y.; Jia, X.; Li, J.; Zhang, M.; Yin, L. Review on the Stability Mechanism and Application of Water-in-Oil Emulsions Encapsulating Various Additives. *Compr. Rev. Food Sci. Food Saf.* **2019**, *18* (6), 1660–1675. https://doi.org/10.1111/1541-4337.12482.

(10) Arab, D.; Kantzas, A.; Bryant, S. L. Nanoparticle Stabilized Oil in Water Emulsions: A Critical Review. *J. Pet. Sci. Eng.* **2018**, *163* (January), 217–242. https://doi.org/10.1016/j.petrol.2017.12.091.

(11) Usaid, A. A. S.; Kumar, P.; Ranganathan, T. V. Emulsion and It's Applications in Food Processing – A Review. *Int. J. Eng. Res. Appl.* **2014**, *4* (4), 241–248.

(12) Tadros, T. F. *Applications of Surfactants in Emulsion Formation and Stabilisation*; 2005. https://doi.org/10.1002/3527604812.ch6.

(13) Ramsden, W. Separation of Solids in the Surface-Layers of Solutions and 'Suspensions' (Observations on Surface-Membranes, Bubbles, Emulsions, and Mechanical Coagulation).—Preliminary Accou. *Proc. R. Soc. London* **1903**, *72* (477–486), 156–162. https://doi.org/https://doi.org/10.1098/rspl.1903.0034.

(14) Pickering, S. U. Emulsions. *J. Chem. Soc. Trans.* **1907**, *91*, 2001–2021. https://doi.org/10.1002/9781119220510.ch15.

(15) Aveyard, R.; Binks, B. P.; Clint, J. H. Emulsions Stabilised Solely by Colloidal Particles. *Adv. Colloid Interface Sci.* **2003**, *100–102*, 503–546. https://doi.org/https://doi.org/10.1016/S0001-8686(02)00069-6.

(16) Binks, B. P.; Yin, D. Pickering Emulsions Stabilized by Hydrophilic Nanoparticles:: In Situ Surface Modification by Oil. *Soft Matter* **2016**, *12* (32), 6858–6867. https://doi.org/10.1039/c6sm01214k.

(17) Wood, T.; Simmons, M. J. H.; Greenwood, R. W.; Turnbull, S. A.; Stitt, E. H. 110th Anniversary : Slurryability: What Makes a Powder Hard To Incorporate into a Slurry? . *Ind. Eng. Chem. Res.* **2019**, *58*, 14396–14409. https://doi.org/10.1021/acs.iecr.9b00572.

(18) Baldovino-Medrano, V. G.; Alcázar, C.; Colomer, M. T.; Moreno, R.; Gaigneaux, E. M. Understanding the Molecular Basics behind Catalyst Shaping: Preparation of Suspensions of Vanadium–Aluminum Mixed (Hydr)Oxides. *Appl. Catal. A Gen.* **2013**, *468*, 190–203. https://doi.org/10.1016/j.apcata.2013.08.041.

(19) Baldovino-Medrano, V. G.; Alcázar, C.; Colomer, M. T.; Moreno, R.; Gaigneaux, E. M. Understanding the Molecular Basics behind Catalyst Shaping: Preparation of Suspensions of Vanadium-Aluminum Mixed (Hydr)Oxides. *Appl. Catal. A Gen.* **2013**, *468*. https://doi.org/10.1016/j.apcata.2013.08.041.

(20) Walther, A.; Müller, A. H. E. Janus Particles: Synthesis, Self-Assembly, Physical Properties, and Applications. *Chem. Rev.* **2013**, *113* (7), 5194–5261. https://doi.org/10.1021/cr300089t.

(21) Rahiminezhad, Z.; Tamaddon, A. M.; Borandeh, S.; Abolmaali, S. S. Janus Nanoparticles: New Generation of Multifunctional Nanocarriers in Drug Delivery, Bioimaiging and Theranostics. *Appl. Mater. Today* **2020**, *18*, 100513. https://doi.org/10.1016/j.apmt.2019.100513.

(22) Kirillova, A.; Schliebe, C.; Stoychev, G.; Jakob, A.; Lang, H.; Synytska, A. Hybrid Hairy Janus Particles Decorated with Metallic Nanoparticles for Catalytic Applications. *ACS Appl. Mater. Interfaces* **2015**, *7* (38), 21224–21225. https://doi.org/10.1021/acsami.5b05224.

(23) Agrawal, G.; Agrawal, R. Janus Nanoparticles: Recent Advances in Their Interfacial and

Biomedical Applications. *ACS Appl. Nano Mater.* **2019**, *2* (4), 1738–1757. https://doi.org/10.1021/acsanm.9b00283.

(24) Su, H.; Hurd Price, C. A.; Jing, L.; Tian, Q.; Liu, J.; Qian, K. Janus Particles: Design, Preparation, and Biomedical Applications. *Mater. Today Bio* **2019**, *4*, 100033. https://doi.org/10.1016/j.mtbio.2019.100033.

(25) Lattuada, M.; Hatton, T. A. Synthesis, Properties and Applications of Janus Nanoparticles. *Nano Today* **2011**, *6* (3), 286–308. https://doi.org/10.1016/j.nantod.2011.04.008.

(26) Luo, D.; Wang, F.; Zhu, J.; Cao, F.; Liu, Y.; Li, X.; Willson, R. C.; Yang, Z.; Chu, C. W.; Ren, Z. Nanofluid of Graphene-Based Amphiphilic Janus Nanosheets for Tertiary or Enhanced Oil Recovery: High Performance at Low Concentration. *Proc. Natl. Acad. Sci. U. S. A.* **2016**, *113* (28), 7711–7716. https://doi.org/10.1073/pnas.1608135113.

(27) Giraldo, L. J. Janus Nanoparticles for Enhanced Oil Recovery EOR: Reduction of Interfacial Tension. *Proc. - SPE Annu. Tech. Conf. Exhib.* **2018**, *2018-Septe*. https://doi.org/10.2118/194033-stu.

(28) Tu, F. Emulsion Stabilization with Janus Particles Emulsion Stabilization with Janus Particles, University of Pennsylvania, 2015.

(29) Pey, C. M.; Maestro, A.; Solé, I.; González, C.; Solans, C.; Gutiérrez, J. M. Optimization of Nano-Emulsions Prepared by Low-Energy Emulsification Methods at Constant Temperature Using a Factorial Design Study. *Colloids Surfaces A Physicochem. Eng. Asp.* **2006**, *288* (1–3), 144–150. https://doi.org/10.1016/j.colsurfa.2006.02.026.

(30) Salager, J. L.; Perez-Sanchez, M.; Garcia, Y. Physicochemical Parameters Influencing the Emulsion Drop Size. *Colloid Polym. Sci.* **1996**, *274* (1), 81–84. https://doi.org/10.1007/BF00658913.

(31) Querol, N.; Barreneche, C.; Cabeza, L. F. Method for Controlling Mean Droplet Size in the Manufacture of Phase Inversion Bituminous Emulsions. *Colloids Surfaces A Physicochem. Eng. Asp.* **2017**, *527* (February), 49–54. https://doi.org/10.1016/j.colsurfa.2017.05.018.

(32) Gingras, J. P.; Tanguy, P. A.; Mariotti, S.; Chaverot, P. Effect of Process Parameters on Bitumen Emulsions. *Chem. Eng. Process. Process Intensif.* **2005**, *44* (9), 979–986. https://doi.org/10.1016/j.cep.2005.01.003.

(33) Frelichowska, J.; Bolzinger, M. A.; Chevalier, Y. Effects of Solid Particle Content on Properties of o/w Pickering Emulsions. *J. Colloid Interface Sci.* **2010**, *351* (2), 348–356. https://doi.org/10.1016/j.jcis.2010.08.019.

(34) Saari, H.; Heravifar, K.; Rayner, M.; Wahlgren, M.; Sjöö, M. Preparation and Characterization of Starch Particles for Use in Pickering Emulsions. *Cereal Chem.* **2016**, *93* (2), 116–124. https://doi.org/10.1094/CCHEM-05-15-0107-R.

(35) Gonzalez Ortiz, D.; Pochat-Bohatier, C.; Cambedouzou, J.; Bechelany, M.; Miele, P. Current Trends in Pickering Emulsions: Particle Morphology and Applications. *Engineering* **2020**, *6* (4), 468–482. https://doi.org/10.1016/j.eng.2019.08.017.

(36) Youssif, M. I.; El-Maghraby, R. M.; Saleh, S. M.; Elgibaly, A. Silica Nanofluid Flooding for Enhanced Oil Recovery in Sandstone Rocks. *Egypt. J. Pet.* **2018**, *27* (1), 105–110. https://doi.org/10.1016/j.ejpe.2017.01.006.

(37) Werner, S.; Fink, A.; Bohn, E. Controlled Growth of Monodisperse Silica Spheres in the Micron

Size Range. *J. Phys. Ther. Sci.* **1968**, *26* (1), 62–69. https://doi.org/10.1016/0021-9797(68)90272-5.

(38) Giermanska-Kahn, J.; Laine, V.; Arditty, S.; Schmitt, V.; Leal-Calderon, F. Particle-Stabilized Emulsions Comprised of Solid Droplets. *Langmuir* **2005**, *21* (10), 4316–4323. https://doi.org/10.1021/la0501177.

(39) Li, W.; Zhang, M.; Zhang, J.; Han, Y. Self-Assembly of Cetyl Trimethylammonium Bromide in Ethanol-Water Mixtures. *Front. Chem. China* **2006**, *1* (4), 438–442. https://doi.org/10.1007/s11458-006-0069-y.

(40) Perro, A.; Meunier, F.; Schmitt, V.; Ravaine, S. Production of Large Quantities of "Janus" Nanoparticles Using Wax-in-Water Emulsions. *Colloids Surfaces A Physicochem. Eng. Asp.* **2009**, *332* (1), 57–62. https://doi.org/10.1016/j.colsurfa.2008.08.027.

(41) Rueden, C. T.; Schindelin, J.; Hiner, M. C.; DeZonia, B. E.; Walter, A. E.; Arena, E. T.; Eliceiri, K. W. ImageJ2: ImageJ for the next Generation of Scientific Image Data. *BMC Bioinformatics* **2017**, *18* (1), 1–26. https://doi.org/10.1186/s12859-017-1934-z.

(42) Brunauer, S.; Emmett, P. H.; Teller, E. Adsorption of Gases in Multimolecular Layers. *J. Am. Chem. Soc.* **1938**, *60* (2), 309–319. https://doi.org/10.1021/ja01269a023.

(43) Thommes, M.; Kaneko, K.; Neimark, A. V.; Olivier, J. P.; Rodriguez-Reinoso, F.; Rouquerol, J.; Sing, K. S. W. Physisorption of Gases, with Special Reference to the Evaluation of Surface Area and Pore Size Distribution (IUPAC Technical Report). *Pure Appl. Chem.* **2015**, *87* (9–10), 1051–1069. https://doi.org/10.1515/pac-2014-1117.

(44) KRUSS. Young-Laplace fit.

(45) Navidi, W. *Statistics for Engineers and Scientists.*, 4th ed.; McGraw Hill, 2015.

(46) Montgomery, D. C. *Design and Analysis of Experiments*, 8th ed.; John Wiley & Sons: New York, 2013.

(47) Caballero, K. V; Guerrero-Amaya, H.; Baldovino-Medrano, V. G. Revisiting Glycerol Esterification with Acetic Acid over Amberlyst-35 via Statistically Designed Experiments: Overcoming Transport Limitations. *Chem. Eng. Sci.* **2019**. https://doi.org/https://doi.org/10.1016/j.ces.2019.06.003.

(48) Pecora., R. Dynamic Light Scattering Measurement of Nanometer Particles in Liquids. *J. ofNanoparticle Res. 2* **2000**, 121–131. https://doi.org/10.1023/A:1010067107182.

(49) Issa, A. A.; Luyt, A. S. Kinetics of Alkoxysilanes and Organoalkoxysilanes Polymerization: A Review. *Polymers (Basel).* **2019**, *11* (3). https://doi.org/10.3390/polym11030537.

(50) Yevchuk, I.; Demchyna, O.; Kopylets, V.; Koval, Z.; Romaniuk, H. Kinetic Regularities of the Early Stages of Sol-Gel Process in Tetraethoxysilane-Based Systems. *Chem. Chem. Technol.* **2014**, *8* (2), 147–155. https://doi.org/10.23939/chcht08.02.147.

(51) Park, S. K.; Kim, K. Do; Kim, H. T. LPreparation of Silica Nanoparticles: Determination of the Optimal Synthesis Conditions for Small and Uniform Particles. *Colloids and Surfaces* **2002**, *197*, 7–17. https://doi.org/10.2147/IMCRJ.S118345.

(52) Silicon dioxide.

(53) Oliveira, R. J.; De Conto, J. F.; Oliveira, M. R.; Egues, S. M. S.; Borges, G. R.; Dariva, C.; Franceschi, E. CO 2 /CH 4 Adsorption at High-Pressure Using Silica-APTES Aerogel as

Adsorbent and near Infrared as a Monitoring Technique. *J. CO2 Util.* **2019**, *32* (October 2018), 232–240. https://doi.org/10.1016/j.jcou.2019.04.019.

(54) Zhang, M.; Moxon, T. Infrared Absorption Spectroscopy of SiO2-Moganite. *Am. Mineral.* **2014**, *99* (4), 671–680. https://doi.org/10.2138/am.2014.4589.

(55) Mirzabe, G. H.; Keshtkar, A. R. Application of Response Surface Methodology for Thorium Adsorption on PVA/Fe3O4/SiO2/APTES Nanohybrid Adsorbent. *J. Ind. Eng. Chem.* **2015**, *26*, 277–285. https://doi.org/10.1016/j.jiec.2014.11.040.

(56) Pretsch, E.; Clerc, J.-T. *Spectra Interpretation of Organic Compounds*; Wiley-VCH, 1997.

(57) Xu, P.; Wang, H.; Tong, R.; Du, Q.; Zhong, W. Preparation and Morphology of SiO 2 /PMMA Nanohybrids by Microemulsion Polymerization. *Colloid Polym. Sci.* **2006**, *284* (7), 755–762. https://doi.org/10.1007/s00396-005-1428-9.

(58) Kosmulski, M. Isoelectric Points and Points of Zero Charge of Metal (Hydr)Oxides: 50 Years after Parks' Review. *Adv. Colloid Interface Sci.* **2016**, *238*, 1–61. https://doi.org/10.1016/j.cis.2016.10.005.

(59) Zenerino, A.; Peyratout, C.; Aimable, A. Synthesis of Fluorinated Ceramic Janus Particles via a Pickering Emulsion Method. *J. Colloid Interface Sci.* **2015**, *450*, 174–181. https://doi.org/10.1016/j.jcis.2015.03.011.

(60) Qiao, B.; Wang, T. J.; Gao, H.; Jin, Y. High Density Silanization of Nano-Silica Particles Using γ-Aminopropyltriethoxysilane (APTES). *Appl. Surf. Sci.* **2015**, *351*, 646–654. https://doi.org/10.1016/j.apsusc.2015.05.174.

(61) Zhuravlev, L. T. The Surface Chemistry of Amorphous Silica. Zhuravlev Model. *Colloids Surfaces A Physicochem. Eng. Asp.* **2000**, *173* (1), 1–38. https://doi.org/https://doi.org/10.1016/S0927-7757(00)00556-2.

(62) Zhang, Y.; Gao, F.; Wanjala, B.; Li, Z.; Cernigliaro, G.; Gu, Z. High Efficiency Reductive Degradation of a Wide Range of Azo Dyes by SiO2-Co Core-Shell Nanoparticles. *Appl. Catal. B Environ.* **2016**, *199* (June), 504–513. https://doi.org/10.1016/j.apcatb.2016.06.030.

(63) Kyaw, H. H.; Al-Harthi, S. H.; Sellai, A.; Dutta, J. Self-Organization of Gold Nanoparticles on Silanated Surfaces. *Beilstein J. Nanotechnol.* **2015**, *6* (1), 2345–2353. https://doi.org/10.3762/bjnano.6.242.

(64) Allouche, J.; Tyrode, E.; Sadtler, V.; Choplin, L.; Salager, J. L. Simultaneous Conductivity and Viscosity Measurements as a Technique To Track Emulsion Inversion by the Phase-Inversion-Temperature Method. *Langmuir* **2004**, *20* (6), 2134–2140. https://doi.org/10.1021/la035334r.

(65) Finkle, P.; Draper, H. D.; Hildebrand, J. H. The Theory of Emulsification. *J. Am. Chem. Soc.* **1923**, *45* (12), 2780–2788. https://doi.org/10.1021/ja01665a002.

(66) Pal, R. Effect of Droplet Size on the Rheology of Emulsions. *AIChE J.* **1996**, *42* (11), 3181–3190. https://doi.org/https://doi.org/10.1002/aic.690421119.

(67) Wu, C. F. J.; Hamada, M. S. *Experiments: Planning, Analysis, and Optimization*, 2nd ed.; John Wiley & Sons: New Jersey, 2009.

(68) Navidi, W. *Statistics for Engineers & Scientists*, 4th ed.; McGraw-Hill Eductation: New York, 2015.

(69) Wagenmakers, E.-J.; Krypotos, A.-M.; Criss, A. H.; Iverson, G. On the Interpretation of

Removable Interactions: A Survey of the Field 33 Years after Loftus. *Mem. Cognit.* **2012**, *40* (2), 145–160. https://doi.org/10.3758/s13421-011-0158-0.

(70) Quinn, G. P.; Keough, M. J. *Experimental Design and Data Analysis for Biologists*, 1st ed.; Cambridge University Press: Cambridge, 2002.

(71) Wagenmakers, E.-J.; Krypotos, Angelos-MiltiadisCriss, A. H.; Iverson, G. On the Interpretation of Removable Interactions: A Survey of the Field 33 Years after Loftus. *Mem Cogn.* **2012**, *40* (2), 145–160. https://doi.org/10.3758/s13421-011-0158-0.

(72) Haney, B.; Chen, D.; Cai, L. H.; Weitz, D.; Ramakrishnan, S. Millimeter-Size Pickering Emulsions Stabilized with Janus Microparticles. *Langmuir* **2019**, *35* (13), 4693–4701. https://doi.org/10.1021/acs.langmuir.9b00058.

(73) Ikem, V. O.; Menner, A.; Bismarck, A.; Norman, L. R. Liquid Screen: A Novel Method to Produce an in-Situ Gravel Pack. *SPE J.* **2014**, *19* (3), 437–442. https://doi.org/10.2118/141256-PA.

(74) Wang, Z.; Wang, Y. Tuning Amphiphilicity of Particles for Controllable Pickering Emulsion. *Materials (Basel).* **2016**, *9* (11). https://doi.org/10.3390/ma9110903.

(75) Danaei, M.; Dehghankhold, M.; Ataei, S.; Hasanzadeh Davarani, F.; Javanmard, R.; Dokhani, A.; Khorasani, S.; Mozafari, M. R. Impact of Particle Size and Polydispersity Index on the Clinical Applications of Lipidic Nanocarrier Systems. *Pharmaceutics*. 2018. https://doi.org/10.3390/pharmaceutics10020057.

(76) Fernandez, J.; Assael, M. J.; Enick, R. M.; Trusler, J. P. M. International Standard for Viscosity at Temperatures up to 473 K and Pressures below 200 MPa (IUPAC Technical Report). *Pure Appl. Chem.* **2019**, *91* (1), 161–172. https://doi.org/doi:10.1515/pac-2018-0202.

(77) Bird, R. B.; Stewart, W. E.; Lightfoot, E. N. *Transport Phenomena*, 1st ed.; John Wiley & Sons: New York, NY, 1960.

(78) Derkach, S. R. Rheology of Emulsions. *Adv. Colloid Interface Sci.* **2009**, *151* (1), 1–23. https://doi.org/https://doi.org/10.1016/j.cis.2009.07.001.

(79) Barnes, H. A. Rheology of Emulsions — a Review. *Colloids Surfaces A Physicochem. Eng. Asp.* **1994**, *91*, 89–95. https://doi.org/https://doi.org/10.1016/0927-7757(93)02719-U.

(80) Celis-Cornejo, C. M.; Pérez-Martínez, D. J.; Orrego-Ruiz, J. A.; Baldovino-Medrano, V. G. Identification of Refractory Weakly Basic Nitrogen Compounds in a Deeply Hydrotreated Vacuum Gas Oil and Assessment of the Effect of Some Representative Species over the Performance of a Ni-MoS2/Y-Zeolite-Alumina Catalyst in Phenanthrene Hydrocracking. *Energy and Fuels* **2018**, *32* (8), 8715–8726. https://doi.org/10.1021/acs.energyfuels.8b02045.

(81) Alomair, O.; Jumaa, M.; Alkoriem, A.; Hamed, M. Heavy Oil Viscosity and Density Prediction at Normal and Elevated Temperatures. *J. Pet. Explor. Prod. Technol.* **2016**, *6* (2), 253–263. https://doi.org/10.1007/s13202-015-0184-8.

(82) Foglino, M.; Morozov, A. N.; Marenduzzo, D. Rheology and Microrheology of Deformable Droplet Suspensions. *Soft Matter* **2018**, *14* (46), 9361–9367. https://doi.org/10.1039/C8SM01669K.

(83) Box, G. E. P.; Hunter, J. S.; Hunter, W. G. *Statistics for Experimenters: Design, Innovation, and Discovery*, 2nd ed.; Wiley-Interscience: New Jersey, 2005.